On the stability of plane viscoelastic shear flows in the limit of infinite Weissenberg and Reynolds numbers

Ahmed Kaffel

Dissertation submitted to the Faculty of the
Virginia Polytechnic Institute and State University
in partial fulfillment of the requirements for the degree of

Doctor of Philosophy
in
Mathematics

Michael Renardy, Chair
Yuriko Renardy
Romesh C. Batra
Saad Ragab
Jeff Borggaard

March 15, 2011
Blacksburg, Virginia

Keywords: Stability of shear flow, inviscid, infinite Weissenberg number limit

On the Stability of plane viscoelastic shear flows in the limit of infinite Weissenberg and Reynolds numbers

(ABSTRACT)

Elastic effects on the hydrodynamic instability of inviscid parallel shear flows are investigated through a linear stability analysis. We focus on the upper convected Maxwell model in the limit of infinite Weissenberg and Reynolds numbers. Specifically, we study the effects of elasticity on the instability of a few classes of simple parallel flows, specifically plane Poiseuille and Couette flows, the hyperbolic-tangent shear layer and the Bickley jet.

The equation for stability is derived and solved numerically using the Chebyshev collocation spectral method. This algorithm is computationally efficient and accurate in reproducing the eigenvalues. We consider flows bounded by walls as well as flows bounded by free surfaces. In the inviscid, nonelastic case all the flows we study are unstable for free surfaces. In the case of wall bounded flow, there are instabilities in the shear layer and Bickley jet flows. In all cases, the effect of elasticity is to reduce and ultimately suppress the inviscid instability. The numerical solutions are compared with the analysis of the long wave limit and excellent agreement is shown between the analytical and the numerical solutions. We found flows which are long wave stable, but nevertheless unstable to wave numbers in a certain finite range. While elasticity is ultimately stabilizing, this effect is not monotone; there are instances where a small amount of elasticity actually destabilizes the flow.

The linear stability in the short wave limit of shear flows bounded by two parallel free surfaces is investigated. Unlike the plane Couette flow which has no short wave instability, we show that plane Poiseuille flow has two unstable eigenmodes localized near the free surfaces which can be combined into an even and an odd eigenfunctions. The derivation of the asymptotics of these modes shows that our numerical eigenvalues are in agreement with the analytic formula and that the difference between the two eigenvalues tends to zero exponentially with the wavenumber α.

Keywords: Stability of shear flow, inviscid, infinite Weissenberg number limit

Dedication

To my mom and dad, Mrs. Souad Abdmouleh and Mr. Abdelhamid Kaffel

To my wife Nihel Charfi.

Acknowledgments

First of all I wish to express my deepest gratitude to Professor Michael Renardy, for conceiving and directing this research project and for the opportunity to contribute to his research in this very stimulating field. Completing this work would have been a difficult task without his continuous guidance and assistance, his unfailing enthusiasm, and his contagious optimism. He has set aside many hours, from his already busy schedule, to share with me some of his expertise.

Thanks also are due to Professors Yuriko Renardy, Jeff Borggaard, Romesh Batra, and Saad Ragab for serving as committee members and to all the Professors in the department for teaching various mathematical tools.

Many thanks go to all my friends in the department for their friendship, good times, and their help discussions and viewpoints.

Thanks are due to my father, Abdelhamid, mother, Souad, my sister, Ines, and my brothers Mohamed and Lassaad for their affection and support over the years and due to my parents in-laws, Riadh and Najoua Charfi for their encouragement and support.

Special thanks are also due to my wife, Nihel, for her inspiration and considerable patience and support over the years.

This work was supported by National Science Foundation under contract DMS-1008426.

Contents

List of Figures

List of Tables

Chapter 1

Introduction

Viscoelastic instabilities are of practical importance, and are a rich subject in fluid mechanics of growing interest. Daily life abounds with examples of complex fluids exhibiting interesting and unexpected flow patterns and complex dynamics even in situations where inertia and surface tension play no role at all. The Newtonian model becomes inadequate for the behavior of these fluids which have a microstructure involving much larger length scales than the atomic scale. By far the most widely and best understood class of non-Newtonian fluids is that of polymeric fluids, and it is this class of fluids which we will study.

Flow instabilities are known to occur in a variety of polymer processing operations. The viscoelastic nature of most polymeric fluids has a variety of complex effects on flow stability. Depending on the particular flow and the fluid's rheology, viscoelasticity can either stabilize or destabilize the flow. We will review many of the known instabilities that occur in polymeric flows and we will describe viscoelasticity in words and in equations.

In section 1 we provide a brief introduction about non-Newtonian fluids, we will describe the important classes of non-Newtonian fluids and the properties of viscoelastic fluids. We will discuss in section 2 the formulation of mathematical equations to model such flows. In section 3, we will present the most important classes of constitutive equations: first the simple rate equations, including the Newtonian constitutive equations and the generalized Newtonian constitutive equations, then the Maxwell models: the upper convected Maxwell, the lower

convected Maxwell, and the corotational Maxwell equations, and finally the Oldroyd-B and other rate equations, including Giesekus and Johnson-Segalman models, which are derived from the upper convected Maxwell model by adding quadratic terms into it. The K-BKZ equation by Kaye, Bernstein, Kearsley, and Zapas (1963) will not be covered in this section. In the following sections we will cover some classes of viscoelastic instabilities, namely instabilities in Taylor-Couette flows and plate-and-plate flows, instabilities in parallel shear flows, and interfacial instabilities in shearing flows. The method of the stability analysis will be also presented. Finally, we will end this chapter by the motivation for which we will study the elastic effects on the stability of plane parallel shear flows of an upper convected Maxwell fluid.

1.1 Newtonian versus non-Newtonian fluids

A Newtonian fluid is a fluid in which the stress is directly proportional to the velocity gradients. Mathematically, the shear force follows a simple Newton's law of viscosity

$$\tau = \mu\dot{\gamma},$$

where τ is the shear stress, μ is the viscosity and $\dot{\gamma}$ is the shear rate. Most fluids of simple structure, composed of relatively simple molecules in a single phase, behave as Newtonian fluids. Some of the examples of Newtonian fluids are water, oil and alcohol.
For a Newtonian fluid, the viscosity depends only on temperature and pressure and also the chemical composition of the fluid if the fluid is not a pure substance, not on the forces acting upon it. For most liquids, the viscosity decreases with temperature and increases with pressure. For gases, it increases with both temperature and pressure. Broadly, the higher is the viscosity of a substance, the more resistance it presents to flow. Table (1.1) provides typical values of viscosity of common fluids. As we go down in the table, the viscosity increases by several order of magnitudes, and thus one can argue that a solid can be treated as a fluid whose viscosity tends to infinity.

Any fluids which do not conform to the Newtonian postulate of the linear relationship be-

Table 1.1: Values of viscosity for common fluids at room temperature

Substance	μ (Pa.s)
Air	10^{-5}
Water	10^{-3}
Ethyl alcohol	$1.2\ 10^{-3}$
Mercury	$1.5\ 10^{-3}$
Olive oil	0.1
Glycerol	1.5
Honey	10
Bitumen	10^{8}
Molten glass	10^{12}

tween the shear stress and the shear rate are variously known as non-Newtonian, non linear, complex or rheologically complex fluids. A non-Newtonian fluid is a fluid whose flow properties differ in any way from those of Newtonian fluids. A distinguishing characteristic of various non-Newtonian fluids is the dependence of the viscosity on the shear rate or the shear rate history. In a Newtonian fluid, the relation between the shear stress and the shear rate is linear, passing through the origin, the constant of proportionality being the coefficient of viscosity. In a non-Newtonian fluid, the relation between the shear stress and the shear rate is different, and can even be time-dependent. Therefore a constant coefficient of viscosity cannot be defined. Many fluids, including polymers, suspensions or slurries of rigid or deformable solid matter, paste or emulsions, some salt solutions are non-Newtonian fluids, as are many commonly found substances such as ketchup, custard, toothpaste, starch suspensions, paint, blood, and shampoo. Non-Newtonian fluids can be classified as:

1.1.1 Time independent fluids

These fluids exhibit a unique relationship between shear rate and shear stress. This relationship is not directly proportional. Three possibilities exist:

1. Viscoplastic or Bingham plastic fluids. These are characterised by the presence of a yield stress: it remains a solid until a certain magnitude of stress is exceeded, then it flows like a fluid. This concept is used in engineering as an approximation to things like mayonnaise, drilling muds and toothpaste where a yield stress exists. In this respect, the material is more like a solid than a liquid. Its associated viscosity is usually known as the plastic viscosity.

2. Pseudoplastic or shear-thinning fluids. Substances and mixtures such as oil-based paint, toothpaste, mayonnaise and quicksand are fairly viscous at first glance, almost gel-like. Under stress, they seem to flow more easily, as observed by stirring a pot of paint, or stepping onto quicksand. Fluids of this type exhibit a decrease in apparent viscosity as the shear rate increases.

3. Dilatant or shear-thickening fluids. These fluids exhibit the opposite behavior of pseudoplastic fluids.The viscosity of such a fluid increases with increasing shear rate. Figure (1.2) shows the variation of apparent viscosity with shear rate for dilatant fluids. Some examples of dilatant fluids are coal slurries, proteins, and potassium silicate.

1.1.2 Time dependent fluids

The apparent viscosity of these fluids is time dependent when they are under a constant and continuous shear rate. They can be further subdivided as:

1. Thixotropic fluids. Food products, such as mayonnaise, and biological fluids, such as synovial fluid, are thixotropic: they decrease in viscosity the longer they are exposed to stress at constant shear rate, but upon rest, they revert to their initial state. Mud exhibits this property, and in earthquake zones liquefaction occurs, causing landslides.

2. Rheotropic fluids. The relatively few fluids which show the negative thixotropy, i.e., their apparent viscosity (or the corresponding shear stress) increases with time of shearing at constant shear rate and fixed temperature are known as rheotropic fluids.

As opposed to thixotropic fluids, external shear fosters the build up of structure in this case. Pastes of gypsum powder, suspensions of Ammonium oleate, of Vanadium pentoxide at moderate shear rates, coal-water slurries and protein solutions exhibit this type of behavior. Figure 1.1 shows the qualitative shear stress- shear rate behavior for thixotropic and rheotropic fluids.

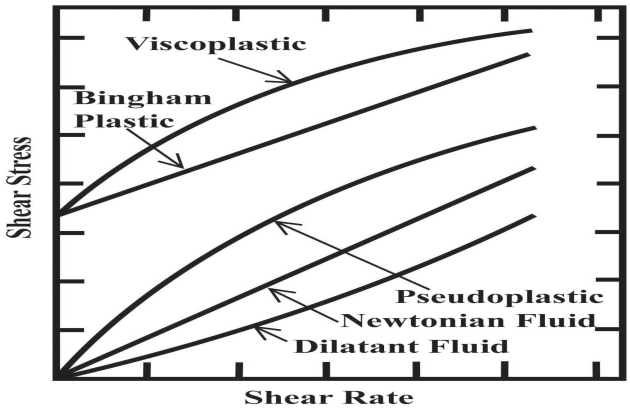

Figure 1.1: Qualitative shear stress- shear rate behavior for thixotropic and rheotropic fluids.

From the thixotropy and rheopexy property displayed by fluids, we see the viscosity may depend on what is happening to them at the present time as well as what has happened to them in the past. The stress and deformation of the body thus depend on time. We might expect that the longer the interval from the present to the past time, the smaller the contribution to the current stress resulting from a given strain in the distant past; this is the principle of fading memory.

1.1.3 Viscoelastic fluids

Materials of this class experience viscosity like a fluid, but also elasticity like a solid. Extremely curious phenomena are observed, for example, the Weissenberg effect (Figure 1.3), self-syphoning (Figure 1.4), and the Barus effect (Figure 1.5). Examples include eggs, magma, glass, oils and blood. Most materials may be considered as viscoelastic, because

they are viscous and elastic up to a certain point, due to the molecular interactions that occur in any sort of matter.

We define a purely viscous fluid to be one whose viscosity is time independent. Figure 1.2 shows typical behavior of various non-Newtonian fluids compared to that of a Newtonian fluid.

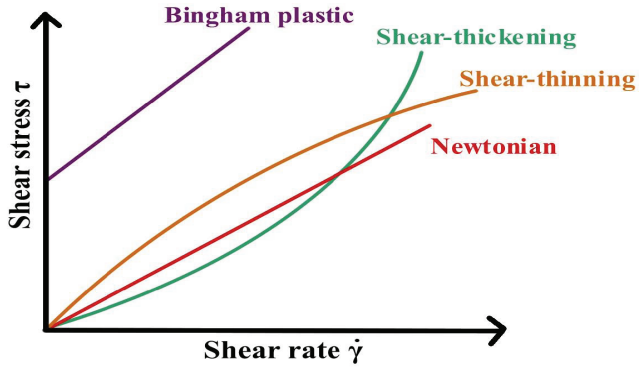

Figure 1.2: A graphical representation of the shear rate-dependent fluids

Viscoelastic materials also exhibit memory since they experience both viscosity and elasticity, so there is a time-dependent deformation associated with them.

Figure 1.3: The Weissenberg or rod-climbing effect. The fluid is high-molecular weight PIB in low molecular weight polyisobutylene. Compare with water, where the swirling effect causes a depression rather than a climbing effect. From Boger and Walters (1993).

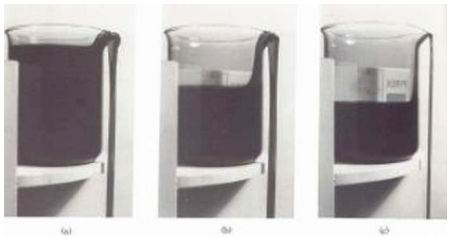

Figure 1.4: The self-syphoning phenomenon. When an aqueous solution of Polyox WSR 301 is spilled over the side, the liquid pours itself out. The pictures are taken after the initial spilling occurs. From Boger and Walters (1993).

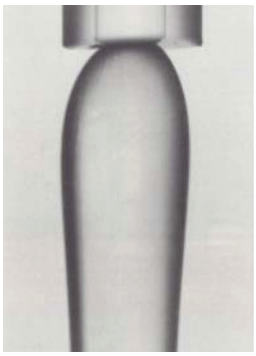

Figure 1.5: When a fluid of aqueous solution of polyacrylamide exits the capillary, it exhibits a swell known as the Barus effect. This is also observed in dyes as well as the Polyox solution in Figure 1.4. From Boger and Walters (1993).

1.1.4 Properties of viscoelastic fluids

It is important to distinguish between dilute solutions and concentrated solutions or melts, because there are profound differences in the rheology of fluids in these two categories that can affect flow stability.

In a shearing flow with the velocity in the direction 1 and the gradient in direction 2, the stress tensor for a viscoelastic fluid can be written in this form:

$$\tau = \begin{pmatrix} \tau_{11} & \tau_{12} & 0 \\ \tau_{21} & \tau_{22} & 0 \\ 0 & 0 & \tau_{33} \end{pmatrix}.$$

The first normal stress difference, $N_1 = \tau_{11} - \tau_{22}$, and the second normal difference, $N_2 = \tau_{22} - \tau_{33}$, are zero for a Newtonian fluid, and the viscosity $\tau_{12}/\dot{\gamma}$ is a constant, where $\dot{\gamma}$ is the shear rate.

Melts and concentrated solutions in shearing flows often have a significant negative second normal stress coefficient [35], while in dilute solutions this quantity can be nearly zero [35]. Thus the stability characteristics of dilute solutions can be profoundly different from those of melts.

The influence of viscoelastic forces on a flow can be characterized by the dimensionless Weissenberg number W. W is the product of the typical velocity gradient and characteristic relaxation time λ. In flows that are time dependent, we can define a Deborah number $De = \lambda/T$, which is the characteristic relaxation for the fluid λ divided by the characteristic time T of the flow. Thus,

$$W = \lambda V/d; \qquad De = \lambda/T,$$

where V is the characteristic velocity and d is the small dimension of the flow geometry so that V/d is a characteristic velocity gradient. T can be either the characteristic time of a flow transient, or the residence time of a fluid particle in the flow.

The Weissenberg number and the Deborah number are frequently proportional to each other, with the constant of proportionality depending on dimensionless geometric or operating parameters of the flow. A high Weissenberg number implies that the first normal stress difference N_1 is larger, or at least comparable in magnitude to the shear stress.

1.2 Mathematical formulation

1.2.1 Equations of motion

In this subsection we provide a brief overview of the mechanics laws. The motion of every fluid is governed by the conservation of mass and momentum, and the energy balance if the thermal effects are important. We assume throughout that the temperature is constant and

that our fluids are incompressible. Hence the mass conservation yields

$$\nabla.v = 0,$$

where v is the velocity of the fluid. In addition, we have the equation of momentum balance

$$\rho\frac{Dv}{Dt} = \nabla.\sigma + F.$$

Here ρ is the density, $\frac{D}{Dt} = \partial_t + v\nabla$ is the material derivative, σ is the stress tensor that represents the forces per unit area of a surface which the material develops in response to being deformed and F can be any body force. For incompressible fluids, the stress tensor is conveniently split into an isotropic piece $-pI$, where p is the isotropic pressure field, and a remainder, here denoted by $T \equiv T_{ij}$, called the deviatoric stress tensor. Thus,

$$\sigma = -pI + T$$

and the momentum equation becomes,

$$\rho\frac{Dv}{Dt} = -\nabla p + \nabla.T + F. \tag{1.1}$$

To complete the mathematical formulation, we need a constitutive law relating the stress T to the motion.

1.2.2 Constitutive laws

We must further specify how the stress tensor T is related to the properties of the fluid. In this subsection, we present the most important classes of constitutive equations:

1. Newtonian constitutive model

The constitutive law for a Newtonian fluid is particularly simple: the deviatoric stress is linearly proportional to the rate of strain and the coefficient of proportionality is the viscosity, μ. The consitutive equation is given by

$$T = 2\mu D, \tag{1.2}$$

In (1.2), D is the rate of strain tensor, which is the symmetric part of the velocity gradient,

$$D = \frac{1}{2}(\nabla v + \nabla v^T).$$

Here we use the convention $(\nabla v)_{ij} = \partial v_i / \partial x_j$. Thus the equation (1.1) reduces to the more familiar Navier-Stokes equation,

$$\rho \frac{Dv}{Dt} = -\nabla p + \mu \nabla^2 v + F. \tag{1.3}$$

2. Generalized Newtonian constitutive model

There are many ways to generalize the linear models by adding non linear terms. In the generalized Newtonian fluids, the extra stress can be expressed as a nonlinear function of the velocity gradient:

$$T = 2\mu(|D|)D, \tag{1.4}$$

where $|D|$ is the norm

$$|D| = (D_{ij}D_{ij})^{1/2}. \tag{1.5}$$

and the viscosity μ is a nonlinear function of $|D|$.

3. Maxwell models

Many Maxwell -type models have been proposed in the literature. In this subsection we restrict ourselves to the the upper convected Maxwell (UCM), the lower convected Maxwell (LCM), and the corotational Maxwell (CRM) models. In viscoelastic fluids, the stress depends not only on the current motion of the fluid, but on the history of the motion. For linear viscoelasticity, Maxwell proposed a linear ordinary differential equation relating the stress T to the velocity gradient

$$\lambda \frac{\partial T}{\partial t} + T = \mu(\nabla v + \nabla v^T),$$

where λ is the relaxation time which represents the time for which the fluid remembers the flow history. This version of Maxwell's model is not frame indifferent (linear models, apart

from the Newtonian fluid, violate frame indifference). We can be solve this differential model and express the stress in the form

$$T(x,t) = \int_{-\infty}^{t} G(t-s)(\nabla v(x,s) + \nabla v^T(x,s))ds,$$

where the stress relaxation modulus G is given by $G(s) = \mu \exp(-s/\lambda)$, where μ is the constant viscosity and λ is the relaxation time

Based on Maxwell's theory of linear viscoelasticity, new nonlinear differential models are derived. As pointed out by Oldroyd, there are natural candidates for a frame indifferent version of Maxwell's theory, the upper convected Maxwell (UCM) model,

$$\lambda(\frac{\partial T}{\partial t} + (v.\nabla)T - (\nabla v)T - T.(\nabla v)^T) + T = 2\mu D, \tag{1.6}$$

and the lower convected Maxwell model,

$$\lambda(\frac{\partial T}{\partial t} + (v.\nabla)T + (\nabla v)^T T + T(\nabla v)) + T = 2\mu D, \tag{1.7}$$

The corotational Maxwell (CRM) model is also a nonlinear extension of the Maxwell's idea.

$$\lambda(\frac{\partial T}{\partial t} + (v.\nabla)T + \frac{1}{2}T(\nabla v - (\nabla v)^T) - \frac{1}{2}(\nabla v - (\nabla v)^T)T) + T = 2\mu D. \tag{1.8}$$

The experimental facts on polymeric liquids as well as molecular theories favor the upper convected Maxwell model. The LCM model is normally rejected as a physical model, even for small deformation rates. The normal stress behavior of this model is not confirmed by experiments. We have included this model only for reason of comparison.

4. Oldroyd-B and other rate equations

The simplest constitutive equation useful for describing dilute solutions at high rates of deformation is the Oldroyd-B equation (1950). In this equation the stress tensor is a linear superposition of a UCM and a Newtonian contribution. It is decomposed into two parts,

$$T = \tau^p + \tau^s, \tag{1.9}$$

where τ^p represents the non-Newtonian tensor responsible for the polymeric contribution to the extra-stress tensor and τ^s is due to the Newtonian solvent

$$\tau^s = 2\mu_s D. \tag{1.10}$$

where μ_s is the solvent viscosity.

The polymeric contribution to the stress tensor satisfies the upper convected Maxwell (UCM) equation:

$$\lambda(\frac{\partial \tau^p}{\partial t} + (v.\nabla)\tau^p - (\nabla v)\tau^p - \tau^p.(\nabla v)^T) + \tau^p = 2\mu_p D, \tag{1.11}$$

where μ_p is the polymeric contribution to the shear viscosity and λ is the polymer relaxation time.

The Oldroyd-B constitutive model can be derived from a molecular model in which the polymer molecule is idealized as an infinitely extensible Hookean spring connecting two Brownian beads [36], it has been shown to give predictions in simple shear flows that are in qualitative agreement with measurements for some Boger fluids [37]. If the solvent term in the Oldroyd-B equation is set to zero, the constitutive equation reduces to the upper-convected Maxwell (UCM) equation and if we neglect the polymeric contribution, we obtain the Newtonian constitutive equation. Thus the upper-convected Maxwell (UCM) equation and the Newtonian constitutive equation are special cases of the Oldroyd-B equations.

One of the limitations of the Oldroyd-B equations for describing dilute solution is that it contains only one single relaxation time, while the fluid actually displays a spectrum of time constants [35]. Both the Oldroyd-B and the upper-convected Maxwell models show a zero second normal stress difference N_2 and no shear thinning. These can be good approximations for dilute solutions, but are not acceptable for melts. The simplest modifications to these models involve the addition of an extra term to produce shear thinning, a bounded extensional viscosity, and/or a non-zero N_2.

A number of popular models differ from the upper convected Maxwell by adding quadratic

terms to the equation, for instance, the Johnson-Segalman model (1977),

$$\lambda(\frac{\partial T}{\partial t} + (v.\nabla)T - (\nabla v)T - T.(\nabla v)^T + \nu(TD + DT)) + T = 2\mu D, \tag{1.12}$$

which adds a term proportional to $TD + DT$ to the left side of equation (1.6), the Phan-Thien-Tanner (PTT) model (1977),

$$\lambda(\frac{\partial T}{\partial t} + (v.\nabla)T - (\nabla v)T - T.(\nabla v)^T + \nu(tr(T))T) + T = 2\mu D, \tag{1.13}$$

which adds a term proportional to $\nu(tr(T))T$, and the Giesekus model (1982),

$$\lambda(\frac{\partial T}{\partial t} + (v.\nabla)T - (\nabla v)T - T.(\nabla v)^T + \nu T^2) + T = 2\mu D, \tag{1.14}$$

which adds a term proportional to T^2 . A major reason for adding such terms is that the UCM model overpredicts stresses at large deformation rates; the other models aim to correct this flaw [23].

An even better, though more complicated, constitutive equation for melts and concentrated solutions is the K-BKZ equation, for which the stress is given as function of a strain tensor C. Sometimes it is useful to describe the viscoelasticity by the equation of the second order fluid where the shear viscosity, the first normal stress coefficient and the second normal stress coefficient are all constants. This second order fluid model is useful because it is valid for most fluids in the limit of slow and slowly varying flows, because it is a simple equation, and because it expresses the stress tensor explicitly in terms of the velocity field [6].

In this section we have only mentioned a few models and for extensive discussion and derivative of these and other models, we refer to [6, 13, 34, 35, 36].

1.3 Review of viscoelastic instabilities

In a typical flow many mechanisms may lead to instability. For example, the effects of viscosity, the inertia, the elasticity, and the boundaries all influence the instability. In this section we review some classes of viscoelastic instabilities, namely instabilities in Taylor-Couette flows, instabilities in cone-and-plate and plate-and-plate flows, instabilities in parallel shear flows, and free surface instabilities in shearing flows.

1.3.1 Instabilities in Taylor-Couette flows

One of the classical problems of hydrodynamic instability in Newtonian fluids is the Taylor-Couette flow problem. In this problem, the fluid is confined in the gap between two concentric cylinders. Rotation of one or both cylinders drives the flow. If the radius of the inner cylinder becomes so much larger than the gap between the cylinders, the flow will be equivalent to the plane Couette flow since the effects of the curvature become negligible. In the absence of viscoelastic effect, inertial effects cause instability leading to Taylor cells. This well known Taylor-Couette instability is produced by the centrifugal forces that tend to fling fluid from the inner cylinder towards the outer [42, 43]. Depending on the flow, and on the constitutive equation, elasticity can either stabilize or destabilize these flows. A theoretical result is that Taylor Couette flow is usually stabilized by negative value of the second normal stress tensor N_2.

Early work on viscoelastic Taylor-Couette flow has focussed on the effect of elasticity on the inertial instability. In 1967, Beard, Davies and Walters analyzed the stability problem of the Taylor-Couette flow. Their results of the upper convected Maxwell fluid show that viscoelasticity has a monotonically destabilizing effect on the inertial instability. In addition, when the Deborah number is increased above a threshold, the solution bifurcates, and a new mode of instability appears. This mode is overstable -i.e. it is time-periodic, and for highly elastic fluids it reduces the critical Taylor number by a factor of 100 below that required for the instability in Newtonian fluids [7]. Even when inertia is completely absent, an oscillating

instability occurs at sufficiently large Weissenberg number. Karlsson et al. (1971) have studied the Taylor-Couette flow with the K-BKZ model. They found that in the small gap limit, the stability is affected by the functions of shear rate that can be obtained from the K-BKZ potential function. Their results are similar to those obtained earlier by Miller and Goddard (1966) for the general corotational model.

In 1989, Haas and Buhler showed that the sequence of transitions that occur as the rotation speed increases depends strongly on the fluid's rheology. For a fluid with relatively constant shear viscosity, they found that the flow changed from purely azimuthal base flow to a stationary Taylor-vortex flow, and then to a time-periodic wavy-cell flow, as the Taylor number was increased. These transitions are similar to those for a Newtonian fluid. However, at Weissenberg number of around 10, a further increase in the rotation speed produced an increase of the irregularity in the shape of the wavy-cells and a decrease in the wavy-cell dimensionless wavenumber from 3.2 to 2 (see Figure 1.6). The prediction of these transitions requires not only the use of realistic constitutive equation, but also nonaxisymmetric and nonlinear stability analysis [48].

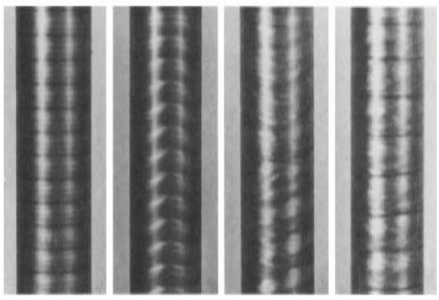

(a) (b) (c) (d)

Figure 1.6: The Taylor-Couette flow for a $500ppm$ solution of polyacrylamide in ethylene glycol. a) Stationary Taylor cells with $\alpha = 3.21$ form at $Ta = 4720$; b) Newtonian-like wavy cells form at $Ta = 11250$; c) tall wavy cells, $\alpha = 1.95$ form at $Ta = 70700$; d) tall stationary cells, $\alpha = 1.95$ appear at $Ta = 151000$

1.3.2 Instabilities in cone-and-plate and plate-and-plate flows

Cone-and-plate and plate-and-plate flows have circular streamlines and are used to measure the normal stresses and the shear viscosities. In the cone-and-plate flow, the vicoelastic fluid is placed in the gap between an inverted cone and a flat plate (see Figure 1.7). Assume that the cone is rotated at a constant angular speed. The resulting flow has important applications in rheometry.

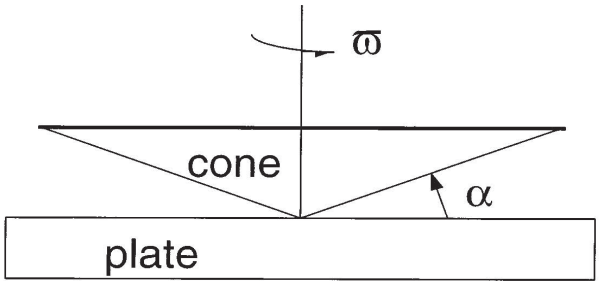

Figure 1.7: The cone-and-plate geometry.

In the plate-and-plate flow a second disk replaces the cone. It is well known that centrifugal effects can produce a secondary flow which becomes significant as the Reynolds number increases. For polymeric liquids, distorsions of the meniscus have often been observed at low Reynolds number. We might observe two types of viscoelastic meniscus distorsion in cone-and-plate and plate-and-plate devices: the irregular, non-axisymmetric distorsion and the axisymmetric indentation of the meniscus. The first type distorsion occurs in etangled polymeric liquids at moderate Weissenberg number and looks like vortices and the second type of an axisymmetric indentation in the meniscus is usually located about halfway between the plate and the cone (or other plate) and is often called fracture [6]. In 1983, Tanner and Keentok showed that an instability to meniscus indentation is observed if the second normal stress difference is negative and large enough.

In experiments with cone-and-plate flow of Boger fluids, McKinley et al. [44] observed that the base torsional flow was stable as long as the Deborah number was not too large. By increasing the Deborah number the base flow became unstable and instead of the steady

azimuthal flow they observed unsteady flow with spiral vortices. At zero Reynolds number, a linear stability analysis of the Oldroyd-B model confirmed the experimental observations [44].

In [45], the effect of inertia on axisymmetric disturbances was analyzed. It was shown that inertia tended to destabilize the flow. Renardy and Olagunju [46] also considered the stability of the flow to non-axisymmetric disturbances when the Reynolds number is non-zero. They examined the inertial effect on the critical value of the Deborah number at the onset of instability, the winding number of the spiral waves, as well as the wave number of the vortices. Their results show that inertia has a stabilizing effect on non-axisymmetric disturbances.

1.3.3 Instabilities in parallel shear flows

The stability of parallel shear flows constitutes a fundamental problem of fluid mechanics. It is an important aspect of studying eventual transition to turbulence, and has been studied for more than a century. We refer to [3, 12, 4] for an overview of the subject in flow instabilities. At high Reynolds number, shear flows can be used in many applications to model all kinds of situations in aero and hydro-dynamics. Boundary layers in pipes, on vehicles etc., shear layer can also model sudden changes in the directions of flow, as are common in the ocean and atmosphere. In many industrial applications, polymers are often added to high Reynolds numbers flows as a strategy to decrease the turbulence. It has been known that the addition of a small amount of polymers reduces the drag of turbulent flow through a pipe; this phenomena is known as turbulent drag reduction. This can enhance pipeline transport, decrease drag and noise production on submarines, stabilize water jets for fire fighting and all kinds of applications like that. The stabilizing effect of elasticity on shear flows is not the primary mechanism of drag reduction, but it is an interesting aspect of these flows. In other contexts, the instabilities may be desirable for example in microfluidics.

Poiseuille flows occur in a variety of polymer shaping processes. At high pressure gradient, a polymer melt shows distorsions. The deleterious effect of these distorsions might be due to

instabilities in viscoelastic parallel shear flows. It is important to understand the combined effects of viscoelasticity and inertia in parallel shear flows, because of their significance in the phenomenon of turbulent drag reduction. Thus, for completeness, we shall here review the effects of both elasticity and inertia on the stability of some parallel shear flows, including channel flows such as plane Couette flow, plane Poiseuille flow, shear layer flow, and Bickley jet flow.

In Newtonian fluids, plane Couette flow has been proved to be stable to waves of all length at all values of the Reynolds number [39], and circular Poiseuille flow is stable at all Reynolds numbers [3], but plane Poseuille flow is unstable to infinitesimal perturbations at a Reynolds number Re of 5772 [38]. There is no instability of the plane Poiseuille flow for any given value of the wavenumber α in the limit of inviscid fluids ($Re = \infty$), by Rayleigh's inflexion-point theorem. Thus while the viscous forces have a stabilizing effect, for the plane Poiseuille flow, viscous forces lead to instabilities. This instability mechanism involves a shift in the phase relationship between the velocity disturbance parallel to the flow and that parallel to flow gradient (Kundo 1990). Hence, it is more subtle than the obvious centrifugal force in the Taylor-Couette instability [6].

A significant literature has studied instabilities in parallel viscoelastic shear flows at finite Reynolds numbers and Weissenberg numbers using analysis, numerics and experiments. The review articles of Renardy [10], by Larson [6] and Shaqfeh [13] are an excellent starting point for further reading. A large number of works have been done on the investigation of the stability of parallel shear flows, including plane Poiseuille and Couette flows.
The problem of the stability of plane Poiseuille flow of viscoelastic fluids at low Reynolds number has been studied by many authors and the flow has been found to be stable [8, 10, 14], in contrast to shear flows with curved streamlines [5, 13]. For high Reynolds number viscoelastic Poiseuille flow, the stability problems have been investigated in [28, 29, 30, 8]. It is shown that viscoelastic effects are destabilizing at high Reynolds number and the critical Reynolds number is decreased by a small amount of elasticity.
The stability analysis by Porteous and Denn using the equation of second order showed that

weak viscoelasticity destabilizes the plane Poiseuille flow to infinitesimal disturbances [30]. That is, the critical Reynolds number for linear instability is reduced by viscoelasticity. To study the effect of strong viscoelasticity, Denn and his coworkers have studied the stability of plane Poiseuille flow of an upper convected Maxwell fluid using a numerical scheme based on the shooting method to determine the most unstable eigenvalue [28, 29, 30]. They found that strong viscoelastic effects are destabilizing at high Reynolds numbers and the critical Reynolds number is decreased. This work shows that as W increases from 0 to 2.28, Re_c decreases from 5772 to 2230. At the same time, the critical wavenumber increases significantly, from $\alpha = 1.02$ to 1.322. At low Reynolds number, no instabilities were found [28], but the numerical method led to artificial instabilities [28, 29].
In a recent study, Sureshkumar, Antony and Beris [14] also employed an efficient algorithm based on Arnoldi orthogonalization to reproduce the most unstable modes. Their results for the UCM model showed a destabilization of the flow at high Reynolds numbers, even for low values of flow elasticity number. These results agreed qualitatively with those reported by Porteus and Denn, although some quantitative differences exist, especially at high values of elasticity.

For plane Couette flow of viscoelastic fluids, it has been found that the Couette flow is stable at low Reynolds numbers [8, 10, 14, 11]. Gorodtsov and Leonov [31] found an exact analytical solution for the case of zero Reynolds number, and thereby proved that the UCM fluid is stable in inertialess plane Couette flow. They also gave an incorrect proof of instability at finite Reynolds numbers. Renardy and Renardy [11] used a spectral method to locate all eigenvalues and showed that Couette flow is stable. They made a few calculations at different values of Weissenberg number, and they found that a small amount of elasticity has a destabilizing effect, but the instability does not occur. The investigation of Lee and Finlayson [8] confirms the absence of instabilities at low Reynolds numbers for the Poiseuille and Couette flows using a similar numerical method, but contradicts "proofs" of instability by Gorodtsov and Leonov [31] and Akbay and Frischmann [32, 33]. The errors in those arguments are pointed out by Renardy [11].

For inviscid flows, shear flows are possible with any velocity profile, and profiles with inflection points lead to inviscid instabilities not present in Couette and Poiseuille flow, see e.g. [3]. A similar limit, in which both the Reynolds and Weissenberg numbers tend to infinity, can be considered for the upper convected Maxwell fluid. Azaiez and Homsy [2] considered a hyperbolic tangent shear layer and Rallison and Hinch [9] considered a submerged jet in this case. They derived an approximate equation and found that elasticity diminishes, but does not entirely suppress the inviscid instability. The flows considered in these papers are unbounded. Recent work by Renardy [10] uses an extension of Howard's semicircle theorem to show that for bounded flows elasticity can entirely suppress inviscid instabilities. Renardy also investigates stability criteria for the long wave limit. The results in [10] concern shear flows bounded by free surfaces as well as wall bounded flows. In the case of free surface flow (without gravity and surface tension), all parallel shear flows with nonconstant profiles are inviscidly unstable. Elasticity can suppress these instabilities.

1.3.4 Free surface instabilities in shearing flows

For flows bounded by free surfaces, there are entire books on stability of films and jets (see [20, 25]), these studies have focussed on instabilities due to surface effects, such as surface tension and air drag, and they usually assume a uniform velocity within the jet or film. Debler and Yue consider an axisymmetric jet bounded by a free surface with a Hagen-Poiseuille profile of the velocity [17]. They conclude that the nonuniform velocity in the jet has a stabilizing effect. This conclusion, however, is due to their failure to consider nonaxisymmetric modes. In [21], it was shown that plane parallel shear flows bounded by two free surfaces have long wave instabilities for all velocity profiles that are not uniform. This is in marked contrast to the wall bounded case, where criteria such as those of Rayleigh and Fjørtoft guarantee stability of a broad class of flows. Other studies consider the effect of viscoelasticity on shear flows with free surfaces. Such flows are common in coating processes, and flow stability is a major practical concern. The stability of films of a viscoelastic fluid on an inclined plane is investigated in [48]. The stress contains a time-dependent memory

term and takes into account the surface tension effect. It is shown that these flows can be stable or unstable depending on the Reynolds number. At high Reynolds number, there is a shear mode of instability that is of Tollmien-Schlichting type [41]. This mechanism occurs at a Reynolds number higher than that necessary to produce a 'surface mode of instability'. Benjamin 1957 and Yih 1963 studied the flow stability of a thin film under the inertial effects to predict when such waves might occur, and thereby to help in the design of methods to avoid them.

The viscoelastic effect might play in the development of these waves, in 1967 Gupta considered the flow of a second order fluid down an inclined surface. The surface area is increased by the formation of surface waves; thus surface tension can be counted on to help stabilize the flow. The longer the wavelength, the less the increase in surface area, and hence the less the stabilizing effect. Thus, by increasing the destabilizing inertial effect until reaching the critical wave growth, one can expect that long waves will be the first to become unstable. This means that the critical wavenumber is usually zero. For a vertical surface, the long waves will grow as a result of either inertial or viscoelastic effects. In [41], Gupta showed that for a viscoelastic flow down a vertical surface the long waves are predicted to grow even at zero Reynolds number, that is a purely viscoelastic mechanism for the instability in gravity-driven film flow. The growth rates of these waves is small when the wavenumber is small. When α is large, however, the second order model does not provide an appropriate description of the viscoelastic effects. To assess the prospect of observing viscoelastic wave formation in the falling film problem, Shaqfeh et al. (1989) extended the analysis to higher wavenumbers. They solved the modified Orr-Somerfeld equation for an Oldroyd-B model for a range of α and We. They found that while viscoelasticity is destabilising at low wavenumber, at higher frequency viscoelasticity is stabilizing. In a film-flow with inertial destabilization, the viscoelasticity can reduce the maximum growth rate and so stabilize the flow.

1.4 Stability analysis

Suppose we have a system with unknowns $\{v, p, T, ..\}$ which could define the velocity, pressure, stress and other fields of the flow. Physically we want to know whether the basic flow can be observed or not. If it is disturbed slightly, the disturbance may either die away or grow. The system is called unstable if there is one such disturbance which causes the system drift away from the original state, it is called stable if all disturbances die away. The case of neutral stability, represented by the marginal states, seperates these two possible cases. One of the main goal in the study of stability is to find the set of marginal states in the phase space we are concerned with. In many practical applications, it is convenient to vary one parameter and keep the others fixed and determine the critical values which give rise to instability.

For our stability analysis, we consider steady flows U, P and S as our solutions in the base flow. We perturb the system a little by adding a sufficiently small disturbances to all the variables. Upon substitution into the full equations of motion and by neglecting quadratic terms we obtain the linearized equations of motions for the disturbances. These equations have coefficients that may vary in space but not time because the basic flow is steady. It follows plausibly that we may separate the variables, so that the general solution is a linear superposition of normal modes, each of the form

$$\widetilde{\mathbf{v}}(x, y, t) = \widetilde{v}(y) \exp(i\alpha(x - ct)),$$

where $\widetilde{v}$ is the amplitude of the disturbance which is a scalar function, α is the wave number, and c is the wave frequency. This may lead to an ordinary-differential, rather than a partial-differential, eigenvalue problem, and thus to a more tractable mathematical problem to solve in order to study the stability problem. The eigenvalues c of this problem are real or occur in complex conjugate pairs.

If $Re(c) > 0$ for a mode, then the disturbance will be amplified, growing exponentially with time until it is so large that nonlinearity becomes significant. $Re(c) < 0$ the mode is said to be stable, and if $Re(c) = 0$ neutrally stable.

Over the next chapters we will study the effect of the elasticity on the stability of some

parallel viscoelastic shear flows. We will see how the elasticity affects the flow stability.

1.5 Motivation

This dissertation is concerned with the linear stability of viscoelastic shear flows of an upper convected Maxwell fluid under the effect of elasticity. We are focused on the stability problem of a few classes of simple parallel flows in the limit of infinite Weissenberg and Reynolds numbers. We will follow up on the work of [10] and discuss the numerical stability results. We shall consider plane Couette and Poiseuille flows, the hyperbolic tangent shear layer, and the Bickley jet flows. For all these flows, we shall consider free surface boundary conditions as well as wall boundary conditions. In the inviscid case, we will show all the flows are unstable for free surfaces. For wall bounded flows, the Couette and Poiseuille flows are stable, while stability of the shear layer and Bickley jet flows depends on the ratio of the channel width to the characteristic length scale of the profile. In all cases, we shall show that elasticity stabilizes and ultimately suppresses the instability. Our numerical approach is based on the Chebyshev collocation spectral method.
We shall also show that some flows, such as plane Poiseuille flow between two parallel free surfaces, also have short wave instabilities. This is in marked contrast to the wall bounded case. In this case, no smooth velocity profiles unstable to short waves are known, and for certain classes of flows there are even results ruling out short wave instability [19, 22].

The dissertation is organized as follow.
In chapter 2, we formulate the governing equations describing the flow of an upper convected Maxwell fluid in the limit where both Reynolds numbers and Weissenberg numbers are infinite. We derive the linearized stability problem and present the extension of Howard's semicircle theorem and some other general stability results. We also discuss the details of the Chebyshev collocation spectral method which is used to solve the linearized stability equation.
In chapter 3, we derive sufficient criteria for long wave instability and the resulting algebraic

equations of the various profiles and we discuss the numerical stability results.

The short wave instability of inviscid plane Poiseuille flow between two parallel free surfaces is also investigated in chapter 4. Unlike the plane Couette flow which has no short wave instability, we will show that plane Poiseuille flow has two unstable eigenmodes localized near the free surfaces.

Finally, we end this dissertation by the conclusions and perspectives.

Chapter 2

Linear perturbation equations for shear flow

2.1 Introduction

In this chapter we discuss and derive the linear perturbation equation to study the stability of plane parallel viscoelastic shear flows.
We first summarize the principles of linear stability analysis. Then we introduce the governing system of equations as well as the boundary conditions and derive the linearized stability problem. We also present the modal solutions and briefly discuss the structure of the continuous and discrete parts of the spectrum. Finally, we discuss the numerical method used to solve the linearized equation.

2.2 Governing system of equations

The system of equations describing the flow of an upper Maxwell fluid is given by

$$\rho(\frac{\partial \boldsymbol{v}}{\partial \boldsymbol{t}} + (\boldsymbol{v}.\nabla)\boldsymbol{v}) = div(\boldsymbol{T}) - \nabla \boldsymbol{p}, \tag{2.1}$$

$$\lambda(\frac{\partial \boldsymbol{T}}{\partial \boldsymbol{t}} + (\boldsymbol{v}.\nabla)\,\boldsymbol{T} - (\nabla \boldsymbol{v})\,\boldsymbol{T} - \boldsymbol{T}(\nabla \boldsymbol{v})^T) = -\boldsymbol{T} + \eta(\nabla \boldsymbol{v} + (\nabla \boldsymbol{v})^T), \tag{2.2}$$

and

$$div(\boldsymbol{v}) = 0, \tag{2.3}$$

where ρ is the density, η is the viscosity, and λ is the relaxation time. In stating these equations, we have followed the following convention

$$(\nabla \boldsymbol{v})_{ij} = \frac{\partial \boldsymbol{v}_i}{\partial \boldsymbol{x}_j}.$$

The bold letters represent dimensional quantities and the coordinate system is chosen such that $\mathbf{x}$ represents the streamwise direction, $\mathbf{y}$ is the normal direction and $\mathbf{z}$ is the spanwise direction.

We are interested in small perturbations of shear flow in the strip $-L < \mathbf{y} < L$.

It is convenient, as usual, to write the governing equations in terms of dimensionless quantities, and for this purpose we introduce a characteristic length L and a characteristic velocity V associated with the basic flow. The choice of L and V is, of course, not unique; we usually take $V = \max|\,U(y)|$, $y_1 \leq y \leq y_2$ and $L = \frac{1}{2}(y_2 - y_1)$.

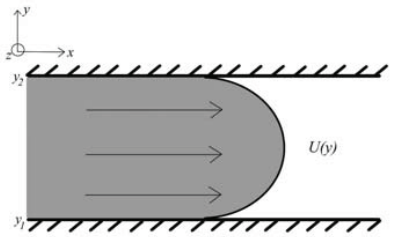

Figure 2.1: Shear flow in the strip $y_1 \leq y \leq y_2$

If we now let

$$t = \boldsymbol{t}V/L, \quad x = \boldsymbol{x}/L, \quad v = \boldsymbol{v}/V, \quad p = \boldsymbol{p}/\rho V^2, \quad U = \boldsymbol{p}/V, \quad T = \boldsymbol{T}/(\frac{\mu V}{L}),$$

where ρ is the (constant) density of the fluid, then the governing equations (2.1)-(2.3) become

$$R(\frac{\partial v}{\partial t} + (v.\nabla)v) = div(T) - \nabla p, \tag{2.4}$$

$$W(\frac{\partial T}{\partial t} + (v.\nabla)T - (\nabla v)T - T(\nabla v)^T) = -T + (\nabla v + (\nabla v)^T), \tag{2.5}$$

and

$$div(v) = 0. \tag{2.6}$$

Here $R = \rho U/\eta$ is the Reynolds number, and $W = \lambda U/L$ is the Weissenberg number, which is a dimensionless measure of the importance of elasticity.

We are interested in studying the asymptotic behavior of solutions in the limit where both Reynolds and Weissenberg numbers are infinite. In this case, we can formally neglect the right hand side in the equation (2.5). Since normal stresses in shear flow are of order W rather than order 1, we shall also scale the stresses with an additional factor W. We obtain the set of equations

$$\frac{\partial v}{\partial t} + (v.\nabla)v = E(div(T) - \nabla p), \tag{2.7}$$

$$\frac{\partial T}{\partial t} + (v.\nabla)T - (\nabla v)T - T(\nabla v)^T = 0, \tag{2.8}$$

and

$$div(v) = 0. \tag{2.9}$$

Where $E = W/R$ is called the elasticity number. These equations have the same status for high Weissenberg number flows that the Euler's equations have for high Reynolds number flows.

2.3 Boundary conditions

As will become evident below, we cannot impose the no slip boundary condition on these reduced equations. As for the Euler equations, only one boundary condition can be imposed. We shall focus on the cases of walls

$$v(x,-1,t) = v(x,1,t) = 0, \tag{2.10}$$

or free surfaces

$$p(x,-1,t) - T_{22}(x,0,t) = p(x,1,t) - T_{22}(x,1,t) = 0. \tag{2.11}$$

Here the free surface condition is imposed at the undeformed interface, which is appropriate for linear perturbations.

2.4 Steady simple shear flow

In this section, the stress tensor in simple shear flow is predicted by the upper convected Maxwell model in the limit where both Reynolds and Weissenberg numbers are infinite.
In the steady simple shear flow, the flow is two dimensional and the velocity is unidirectional $\mathbf{U} =< U(y), 0, 0 >$.
Consequently, the velocity gradient is the matrix

$$\begin{pmatrix} 0 & U'(y) & 0 \\ 0 & 0 & 0 \\ 0 & 0 & 0 \end{pmatrix}.$$

The quantity $U'(y)$ corresponds to the shear rate.
Let $\mathbf{x} =< x, y, z >$ denote the position at time t of the fluid particle which occupies the position $< x - U(y)(t-s), y, z >$ at time s.
The relative deformation gradient is the matrix given by

$$F(\mathbf{x},t,s)=\begin{pmatrix}1 & -U'(y)(t-s) & 0\\ 0 & 1 & 0\\ 0 & 0 & 1\end{pmatrix}.$$

The relative Cauchy strain is defined by

$$C(\mathbf{x},t,s)=F^T(\mathbf{x},t,s)F(\mathbf{x},t,s),$$

which implies

$$C(\mathbf{x},t,s)=\begin{pmatrix}1 & -U'(y)(t-s) & 0\\ -U'(y)(t-s) & 1+U'^2(y)(t-s)^2 & 0\\ 0 & 0 & 1\end{pmatrix}.$$

In general, the stress in a viscoelastic fluid depends on the history of the relative deformation gradient, i.e., $\mathbf{T}$ is a function of all values of $F(\mathbf{x},t,s)$ for times s prior to t. A consequence of material frame difference is that the stress tensor depends on the relative Cauchy strain [23]. That is, we have

$$T(\mathbf{x},t)=g(C(\mathbf{x},t,s))^t_{-\infty},$$

Moreover, this dependence is isotropic

$$g(Q(t)C(\mathbf{x},t,s)Q^{-1}(t))^t_{-\infty}=Q(t)g(C(\mathbf{x},t,s))^t_{-\infty}Q^{-1}(t),$$

for any orthogonal matrix $Q(t)$. If we choose $Q(t)$ to be 180^0 rotation about the z-axis, as shown in [23], it is found that $C(\mathbf{x},t,s)$ and $T(\mathbf{x},t,s)$ are preserved under this transformation, and consequently the components T_{13} and T_{23} are zero. Hence the stress tensor in simple shear flow has the form

$$T=\begin{pmatrix}T_{11} & T_{12} & 0\\ T_{12} & T_{22} & 0\\ 0 & 0 & T_{33}\end{pmatrix}.$$

We shall now consider the limit of infinite Weissenberg and Reynolds numbers. In this case, the upper convected Maxwell model is reduced to equation (2.8). For steady simple shear flow, this leads to

$$T_{12} = T_{22} = T_{33} = 0,$$

and the stress tensor has the form

$$T = \begin{pmatrix} T_{11} & 0 & 0 \\ 0 & 0 & 0 \\ 0 & 0 & 0 \end{pmatrix}.$$

In the next section, we will consider a parallel two-dimensional flow in the x-y plane and the steady stress tensor will be of the form

$$T = \begin{pmatrix} S(y) & 0 \\ 0 & 0 \end{pmatrix}.$$

2.5 The linearized stability problem

To understand the mechanisms controlling the stability of shear flows, we apply a linear stability analysis and consider the eigenvalues of the linearized equations for the perturbation. The flow is assumed to be bounded by the two planes which may be either wall or free surfaces. On a free boundary the pressure must be constant and on a rigid boundary the normal component of the velocity must vanish.

For a parallel two-dimensional flow, the basic steady flow is of the form

$$\boldsymbol{U} = U(y)\boldsymbol{i}, \qquad \boldsymbol{T} = \begin{pmatrix} S(y) & 0 \\ 0 & 0 \end{pmatrix} \quad (y_1 \leq y \leq y_2),$$

where $\boldsymbol{i}$ denotes a unit vector in the x direction.

The coordinate system is chosen such that x represents the streamwise direction, y is the direction normal to the plates and z is the spanwise direction.

The basic flow automatically satisfies both of the boundary conditions and equations (2.7)-(2.9) for any arbitrary distributions $U(y)$ and $S(y)$ of the velocity and the stress with either wall or free surface boundary conditions. In our subsequent analysis, we shall, however, assume that U and S are linked by the viscometric relation

$$S(y) = 2U'(y)^2. \tag{2.12}$$

To study the stability we let

$$p = exp(i\alpha(x - ct))q(y), \tag{2.13}$$

$$\mathbf{v} = (U(y), 0) + exp(i\alpha(x - ct))(u(y), v(y)), \tag{2.14}$$

$$\mathbf{T} = \begin{pmatrix} S(y) & 0 \\ 0 & 0 \end{pmatrix} + exp(i\alpha(x - ct)) \begin{pmatrix} T_{11}(y) & T_{12}(y) \\ T_{12}(y) & T_{22}(y) \end{pmatrix}. \tag{2.15}$$

where $U(y)$ is the is the velocity and $S(y)$ is the normal stress in the base flow. The condition $S(y) \geq 0$ is required since only positive definite stresses are physically attainable for the upper convected Maxwell Model.

On substituting these expressions into (2.7), (2.8) and (2.9) and neglecting quadratic terms in the perturbations, we then obtain the following linearized system of equations for the disturbance

$$i\alpha(U(y) - c)u + U'(y)v - Ei\alpha(T_{11} - q) - ET'_{12} = 0, \tag{2.16}$$

$$i\alpha(U(y) - c)v - Ei\alpha T_{12} - E(T'_{22} - q') = 0, \tag{2.17}$$

$$i\alpha u + v' = 0, \tag{2.18}$$

$$i\alpha(U(y) - c)T_{11} + S'(y)v - 2S(y)i\alpha u - 2U'(y)T_{12} = 0, \tag{2.19}$$

$$i\alpha(U(y) - c)T_{12} - S(y)i\alpha v - U'(y)T_{22} = 0, \tag{2.20}$$

$$i\alpha(U(y)-c)T_{22}=0. \tag{2.21}$$

Here differentiation with respect to y is denoted by a prime. By using the equations (2.20) and (2.21), we have this relation

$$(U(y)-c)T_{12}-S(y)v=0. \tag{2.22}$$

We differentiate (2.17) we obtain:

$$i\alpha(U(y)-c)v'+i\alpha U'v-Ei\alpha T'_{12}-ET"_{22}+Eq"=0. \tag{2.23}$$

By (2.16) and (2.18) we get

$$2\alpha^2(U-c)u-E\alpha^2T_{11}+E\alpha^2q-ET"_{22}+Eq"=0. \tag{2.24}$$

Then we differentiate twice the equation (2.21), we get:

$$(U-c)^2T"_{22}=2U'T_{22}. \tag{2.25}$$

By equations (2.23), (2.24), (2.57), (2.19) and (2.20) we can eliminate variables and reduce this system of equations to the following single equation as it is found in [10]

$$F(y,c)(q''(y)-\alpha^2q)-F'q'=0, \tag{2.26}$$

where

$$F(y,c)=ES(y)-(U(y)-c)^2. \tag{2.27}$$

For boundaries, this being the usual case, we impose the boundary condition

$$q'=0 \ \ at \ \ y=\pm1, \tag{2.28}$$

for walls and

$$q = 0 \ \ at \ \ y = \pm 1, \tag{2.29}$$

for free surfaces.

We note that the elimination process leading to (2.26) concerns discrete eigenmodes and "sweeps under the rug" continuous spectra given by $i\alpha(U(y) - c) = 0$, which are associated with the stress variables. Stress modes associated with these continuous spectra lead to non-normal (algebraic) growth [25, 26, 27]. This will not be further considered in this study, where we limit our attention to exponential instabilities associated with discrete eigenvalues. We note that an analogous decoupling is not possible at finite Weissenberg number, where the inaccurate numerical approximation of continuous spectra is a serious issues [8, 11, 14]. The reduced stability equation derived above still has a continuous spectrum given by $F = 0$, and some care is necessary to distinguish discrete eigenvalues from inaccurate numerical approximations of this continuous spectrum.

If $E = 0$, then equation (2.26) and the boundary conditions reduce to the eigenvalue problem for inviscid parallel shear flows. Note that the equation and the boundary conditions are unchanged when α is replaced by $-\alpha$. Thus without loss of generality, we can take $\alpha \geq 0$, and the criterion for instability then becomes that there exists a solution with $c_i > 0$ for some $\alpha > 0$. If $\alpha c_i > 0$ the disturbance grows exponentially; for negative αc_i we encounter exponential decay.

By solving the initial value problem (2.26)-(2.28) for the variable $q(y)$, the other disturbances variable u and v can be found from the linearized system of equations for the disturbance (2.16)-(2.21).

From equation (2.21), we obtain

$$T_{22} = 0, \tag{2.30}$$

which implies also

$$T'_{22} = 0. \tag{2.31}$$

From (2.20), we get

$$T_{12}(U - c) = Sv. \tag{2.32}$$

Upon substitution of (2.30) and (2.32) into (2.17), we obtain

$$i\alpha F v = E(U-c)q', \tag{2.33}$$

which leads to

$$\frac{v}{E} = \frac{E(U-c)q'}{i\alpha F}. \tag{2.34}$$

Now, we differentiate (2.32), we get

$$(U-c)^2 T_{12}' = (S'v + Sv')(U-c) - SvU'. \tag{2.35}$$

Multiplying equation (2.16) by $(U-c)^2$ we obtain

$$i\alpha(U(y)-c)^3 u + U'(y)(U-c)^2 v - Ei\alpha(U-c)^2 T_{11} + Ei\alpha(U-c)^2 q - E(U-c)^2 T_{12}' = 0. \tag{2.36}$$

Upon substitution of (2.32) into equation (2.19), we have

$$i\alpha(U-c)T_{11} = -S'v + 2i\alpha uS + 2U'\frac{Sv}{U-c}. \tag{2.37}$$

On substituting the relations (2.37), (2.34) and (2.35) into equation (2.36), we obtain

$$i\alpha(U(y)-c)^3 u + \frac{U'(U-c)^2 Eq'}{i\alpha F} - 2Ei\alpha(U-c)Su - EU'Sv + Ei\alpha(U-c)^2 q - ESv'(U-c)^2 = 0. \tag{2.38}$$

Then equations (2.18) and (3.1) give

$$i\alpha uF(U(y)-c) = \frac{E(U-c)^3 U'q'}{i\alpha F} - ESU'v + Ei\alpha q(U-c)^2 = 0. \tag{2.39}$$

Finally, by (2.34) and (2.39) we get

$$\frac{u}{E} = \frac{1}{\alpha^2 F}(U'q' + \alpha^2 q(U-c)). \tag{2.40}$$

2.6 An extension of Howard's semicircle theorem

Howard's semicircle theorem was extended to magnetohydrodynamic flows by Hughes and Tobias [49] and to viscoelastic shear flows by Renardy [10], who proved that the complex

wave velocity for any unstable mode lies within a semi-circle. In the following, we will discuss the spectrum distribution of the disturbances and present the extension of the semi-circle theorem for the unstable perturbation as shown in [10].

Assume c is a non-real eigenvalue. Then we multiply (2.26) by the complex conjugate $\overline{q}$ and integrate over the domain $[-1, 1]$ to give:

$$\int_{-1}^{1}((\frac{q'}{F})' - \frac{\alpha^2}{F}q)\overline{q}dy = 0. \tag{2.41}$$

The first term can be integrated by parts, giving

$$\int_{-1}^{1}((\frac{q'}{F})')\overline{q}dy = \frac{q'\overline{q}}{F}|_0^L - \int_0^L \frac{q'}{F}\overline{q'}dy. \tag{2.42}$$

After applying the boundary conditions (2.29) and using (2.42), the equation (2.41) becomes

$$\int_{-1}^{1}\frac{1}{F}(|q'|^2 + \alpha^2|q|^2)dy = 0. \tag{2.43}$$

By separating the real and imaginary parts of (2.43) we get two equations, namely

$$\int_{-1}^{1}(ES - (U - c_r)^2 + c_i^2)Q^2dy = 0, \tag{2.44}$$

and

$$c_i\int_{-1}^{1}(U - c_r)Q^2dy = 0, \tag{2.45}$$

where

$$Q^2 = \frac{|q'|^2 + \alpha^2|q|^2}{|F|^2}.$$

From this last expression we can infer that either c_i is zero or the integral must vanish. If c_i is zero, we might expect exceptional neutral solution, but the very existence of the integral becomes questionable. When c_i is not zero, we see that the only way for the integral to vanish is for $U - c_r$ to change sign somewhere in the domain.

Hence $U_{min} < c_r < U_{max}$.

If we assumed a non real eigenvalue, the equation (2.45) can be rewritten as

$$\int_0^L UQ^2dy = c_r\int_0^L Q^2dy. \tag{2.46}$$

After substituting into (2.44) we find that

$$\int_0^L U^2 Q^2 dy = \int_0^L (ES + c_r^2 + c_i^2) Q^2 dy. \tag{2.47}$$

For this last expression to be true, the term $U^2 - (ES + c_r^2 + c_i^2)$ must vanish and change sign somewhere in the domain, that is,

$$U_{min}^2 < ES + c_r^2 + c_i^2 < U_{max}^2. \tag{2.48}$$

By noting that

$$(U - U_{min})(U - U_{max}) < 0, \tag{2.49}$$

Where the first term is non-negative and the second term is non-positive, the product being negative or zero. Multiplying by Q^2 and integrating we get

$$\int_{-1}^1 (U - U_{min})(U - U_{max}) Q^2 dy < 0, \tag{2.50}$$

or,

$$\int_{-1}^1 [U^2 - (U_{min} + U_{max})U + U_{min}U_{max}] Q^2 dy < 0 \tag{2.51}$$

The Substitution of the two equalities (2.46) and (2.47) into this inequality gives

$$\int_{-1}^1 [ES + c_r^2 + c_i^2 - (U_{min} + U_{max})c_r + U_{min}U_{max}] Q^2 dy < 0. \tag{2.52}$$

Since Q^2 is positive, the integrand must be negative or

$$ES + c_r^2 + c_i^2 - (U_{min} + U_{max})c_r + U_{min}U_{max} < 0. \tag{2.53}$$

After rearranging terms, (2.53) can be written as

$$(c_r - \frac{U_{min} + U_{max}}{2})^2 + c_i^2 < (\frac{U_{max} - U_{min}}{2})^2 - ES_{min}. \tag{2.54}$$

This is the equation of a semicircle with raduis $((\frac{U_{max} - U_{min}}{2})^2 - ES_{min})^{1/2}$ and c must lie inside the semicircle in order to be a non-real eigenvalue.

For the Newtonian case $E = 0$, this is the Howard's semicircle theorem for inviscid parallel shear flow which gives a simple bound on the location of any unstable eigenvalue. Given a base profile U and an unstable mode with complex wavespeed $c = c_r + ic_i$, the location of c in the complex plane is within the upper half of the circle centered at $(\frac{U_{max}+U_{min}}{2})$ with raduis $(\frac{U_{max}-U_{min}}{2})$.

When $ES_{min} \geq (\frac{U_{max}+U_{max}}{2})^2$ or if ES sufficiently large, the semicircle dissappears, and unstable eigenvalues cannot exist. This result has a nice physical interpretation in terms of the elastic wave speed $\sqrt{ES}$: Inviscid instabilities are suppressed if the maximum difference in velocities is less than twice the minimum elastic wave speed. This precludes a resonant interaction between forward and backward traveling waves [10].

2.7 Stability characteristics of some flows

Now that we have derived general stability criteria for unspecified velocity profiles, we will compute the eigenvalues and the solutions of the eigenvalue problem for simple base flows. We will present two classical examples that will demonstrate the essential features of inviscid stability theory before we move on to numerics. In this section, we derive the analytic dispersion relation and the eigenvalues. The stability of the plane Couette and plane Poiseuille flows with free surface boundary conditions will be investigated. We shall show that the plane Couette flow has no short wave instabilities and the unstable modes exist only in the long wave limit. In contrast, the plane Poiseuille flow has unstable modes in the long and short wave limits. All the details about the short wave instabilities will be discussed in chapter 3.

2.7.1 Couette flow

As a first example of linear velocity profile we consider the stability problem of the plane Couette flow.

For $U(y) = y$, the linear stability equation takes the form

$$(2E - (y-c)^2)(q'' - \alpha^2 q) + 2(y-c)q' = 0, \tag{2.55}$$

which has to be solved subject to the free surface boundary conditions

$$q = 0 \ \ at \ \ y = \pm 1. \tag{2.56}$$

We set

$$z = \frac{y-c}{(2E)^{1/2}}.$$

Using this transformation, the differential equation (2.55) reduces to

$$q'' - \frac{2z}{z^2-1}q' - 2E\alpha^2 q = 0, \tag{2.57}$$

that is of the form

$$q'' + \frac{2(\gamma+1)z}{z^2-1}q' + \frac{4\delta z^2 - \nu}{z^2-1}q = 0. \tag{2.58}$$

This differential equation is obtained from the Heun's Confluent equation

$$q'' - \frac{-az^2 + (-2-\beta-\gamma+a)z + 1 + \beta}{z(z-1)}q' - \frac{((-\beta-\gamma-2)a - 2\delta)z + (\beta+1)a - (\gamma+1)\beta - \gamma - 2\eta}{2z(z-1)}q = 0 \tag{2.59}$$

by taking $a = 0, \beta = -1/2, \eta = (1-\gamma-\nu)/4$ and changing z to z^2. Note that the solution of the Heun's Confluent equation (2.59) is denoted by $HeunC(a, \beta, \gamma, \delta.\eta, z)$.
By identification of the coefficients of the equations (2.59) and (2.59), we find

$$\gamma = -2, \delta = -\frac{E\alpha^2}{2}, \nu = -2E\alpha^2.$$

Hence, we obtain these coefficients

$$a = 0, \beta = -\frac{1}{2}, \gamma = -2, \delta = -\frac{E\alpha^2}{2}, \eta = \frac{3}{4} + \frac{E\alpha^2}{2},$$

and the general solution of the equation (2.55), consistent with the the Maple output, is found to be

$$q(y) = C_1 Q_1(y, c, \alpha, E) + C_2 Q_2(y, c, \alpha, E), \tag{2.60}$$

for some constants C_1 and C_2, where

$$Q_1(y,c,\alpha,E) = HeunC(0,-\frac{1}{2},-2,-\frac{E\alpha^2}{2},\frac{3}{4}+\frac{E\alpha^2}{2},\frac{(y-c)^2}{2E}), \tag{2.61}$$

and

$$Q_2(y,c,\alpha,E) = HeunC(0,\frac{1}{2},-2,-\frac{E\alpha^2}{2},\frac{3}{4}+\frac{E\alpha^2}{2},\frac{(y-c)^2}{2E})y. \tag{2.62}$$

Now the free surface boundary condition applied at $y = \pm 1$ give

$$Q_1(1,c,\alpha,E)C_1 + Q_2(1,c,\alpha,E)C_2 = 0, \tag{2.63}$$

and

$$Q_1(-1,c,\alpha,E)C_1 + Q_2(-1,c,\alpha,E)C_2 = 0. \tag{2.64}$$

Both unknown coefficients C_1 and C_2 can be eliminated from these equations leaving us with a condition on the eigenvalue c of the form

$$\begin{vmatrix} Q_1(1,c,\alpha,E) & Q_2(1,c,\alpha,E) \\ Q_1(-1,c,\alpha,E) & Q_2(-1,c,\alpha,E) \end{vmatrix} = 0.$$

Hence we find the dispersion relation

$$Q_1(1,c,\alpha,E)Q_2(-1,c,\alpha,E) - Q_1(-1,c,\alpha,E)Q_2(1,c,\alpha,E) = 0. \tag{2.65}$$

For the Newtonian case $E = 0$, the stability equation (3.4) becomes

$$(y-c)(q'' - \alpha^2 q) - 2q' = 0. \tag{2.66}$$

The general solution of this equation is

$$q(y) = A_c(-1+\alpha(y-c))\exp(\alpha y) + B_c(1+\alpha(y-c))\exp(-\alpha y), \tag{2.67}$$

for some constants A_c and B_c.
By inserting this into the boundary conditions, we find

$$(-1+\alpha(1-c))\exp(\alpha)A_c + (1+\alpha(1-c))\exp(-\alpha)B_c = 0 \tag{2.68}$$

and

$$(-1+\alpha(1-c))\exp(-\alpha)A_c + (1-\alpha(1+c))\exp(\alpha)B_c = 0 \tag{2.69}$$

It is next a simple matter to eliminate A_c and B_c from these two linear homogeneous equations, by finding that

$$\begin{vmatrix} (-1+\alpha(1-c))\exp(2\alpha) & (1+\alpha(1-c)) \\ -(1+\alpha(1+c)) & (1-\alpha(1+c))\exp(2\alpha) \end{vmatrix} = 0,$$

and hence deducing the eigenvalue relation

$$c^2 = \frac{(1-\alpha)^2\exp(4\alpha) - (1+\alpha)^2}{\alpha^2(\exp(4\alpha)-1))}, \tag{2.70}$$

which is equivalent to

$$c^2 = 1 + \frac{1}{\alpha^2} - \frac{2}{\alpha\tanh(2\alpha)}. \tag{2.71}$$

This relation can also be found from the dispersion equation (2.65) upon substituting of $E = 0$ into it. This gives a pair of neutrally stable waves propagating in opposite direction if $c^2 > 0$ and a pair of stationary modes, one amplified and one damped, if $c^2 < 0$. Taking α_c as the unique positive zero of $(1-\alpha)^2\exp(4\alpha) - (1+\alpha)^2$, we find that $\alpha_c \simeq 1.19968$ and deduce that the mode is unstable if and only if $0 < \alpha < \alpha_c$.

In the long wave limit $\alpha \to 0$, the power series expansion of the right hand side of (2.70) give

$$c^2 = -1/3 + \frac{16}{45}\alpha^2 - \frac{128}{945}\alpha^4 + O\left(\alpha^5\right).$$

This means we encounter two conjugate eigenvalues $c = \pm\frac{i}{\sqrt{3}}$ as $\alpha \to 0$ and the flow will be unstable.

In the short wave limit $\frac{1}{\alpha} \to 0$, the relation (2.71) leads to $c^2 = 1$ which show that all the eigenvalues are real and the flow will be stable.

2.7.2 The plane Poiseuille flow

For plane Poiseuille flow, we have $U(y) = 1 - y^2$, the linear stability equation (2.26) becomes

$$(8Ey^2 - (1 - c - y^2))(q'' - \alpha^2 q) - (16Ey + 4(1 - c - y^2)y)q' = 0, \tag{2.72}$$

with the boundary conditions

$$q(-1) = q(1) = 0. \tag{2.73}$$

It can be seen that this differential equation has singularities at the points y_c in the domain of flow where $F(y_c, c) = 0$ with $F(y_c, c) = 8Ey^2 - (1 - c - y^2)$. For the Newtonian case, these singularities correspond to the points y_c where $U(y_c) = c$ if $0 \leq c \leq 1$. It will be shown that critical layers are important in solving the initial value problem (2.72) - (2.73) for an inviscid fluid.

In the long wave limit $\alpha \to 0$, the general solution of the equation (2.72) is

$$q(y) = A_1 + B_1(-15 + 30c - 15c^2 + (10 + 40E - 10c)y^2 - 3y^4)y, \tag{2.74}$$

for some constants A_1 and B_1. Now the boundary conditions (2.73) applied at $y = \pm 1$ give

$$\begin{vmatrix} 1 & 40E - 16 + 20c - 15c^2 \\ 1 & -(40E - 16 + 20c - 15c^2) \end{vmatrix} = 0,$$

and hence deducing the eigenvalue relation

$$\frac{16}{15} - \frac{16}{3}E - \frac{8}{3}c + 2c^2 = 0. \tag{2.75}$$

The roots of this quadratic equation are real if $E \geq E_c$ where $E_c = \frac{1}{30}$. For the range of elastic numbers $0 \leq E < E_c$, we encounter two conjugate complex eigenvalues and the flow will be unstable. For the Newtonian case $E = 0$, we find two complex conjugate eigenvalues given by $\frac{2}{3} \pm \frac{2\sqrt{5}i}{15}$.

In the short wave limit $\frac{1}{\alpha} \to 0$, for the Newtonian case $E = 0$, the stability equation becomes

$$(1-c-y^2)(q''-\alpha^2 q)+4yq'=0. \tag{2.76}$$

We set

$$z=\frac{y^2}{1-c}$$

,

Our differential equation (2.76) becomes

$$z(z-1)q''=(\frac{3}{2}z+\frac{1}{2})q'+(\frac{\alpha^2(1-c)z-\alpha^2(1-c)}{4})q. \tag{2.77}$$

Identifying the coefficients of this equation with the Heun's Confluent equation (2.59) yields to

$$a=0,\beta=-\frac{1}{2},\gamma=-3,\delta=-\frac{\alpha^2(1-c)}{4},\eta=1+\frac{\alpha^2(1-c)}{4}$$

This is consistent with the Maple's result which produces the following solution

$$\begin{aligned} q(y) &= A_2 HeunC\left(0,-\frac{1}{2},-3,-\frac{1}{4}\alpha^2(1-c),1+\frac{1}{4}(1-c)\alpha^2,\frac{y^2}{1-c}\right) \\ &+B_2 HeunC\left(0,\frac{1}{2},-3,-\frac{1}{4}\alpha^2(1-c),1+\frac{1}{4}(1-c)\alpha^2,\frac{y^2}{1-c}\right)y. \end{aligned} \tag{2.78}$$

Now the boundary conditions (2.73) applied at $y=\pm 1$ give

$$H_1(c,\alpha)A_2-H_2(c,\alpha)B_2=0, \tag{2.79}$$

$$H_1(c,\alpha)A_2+H_2(c,\alpha)B_2=0. \tag{2.80}$$

Where

$$H_1(c,\alpha)=HeunC\left(0,-\frac{1}{2},-3,-\frac{1}{4}\alpha^2(1-c),1+\frac{1}{4}(1-c)\alpha^2,\frac{1}{1-c}\right),$$

and

$$H_2(c,\alpha)=HeunC\left(0,\frac{1}{2},-3,-\frac{1}{4}\alpha^2(1-c),1+\frac{1}{4}(1-c)\alpha^2,\frac{1}{1-c}\right).$$

To eliminate A_2 and B_2 from these two linear homogeneous equation by finding that

$$\begin{vmatrix} H_1(c,\alpha) & -H_2(c,\alpha) \\ H_1(c,\alpha) & H_2(c,\alpha) \end{vmatrix} = 0,$$

and hence we obtain the following dispersion relation

$$H_1(c,\alpha)H_2(c,\alpha) = 0. \tag{2.81}$$

This relation is still valid in the long wave limit since $H_1(c_1, 0) = H_2(c_2, 0) = 0$ where $c_1 = \frac{2}{3} - \frac{2\sqrt{5}i}{15}$ and $c_2 = \frac{2}{3} + \frac{2\sqrt{5}i}{15}$ are the solutions of the quadratic equation (2.75).

2.8 Numerical method

We use a Chebyshev collocation spectral method to solve the linear eigenvalue problem. The algorithm will give consistent results with asymptotic results both in the short and long wave limit.

In this section we describe the details of the implementation of the numerics we use in the computation of eigenvalues for the stability problem. The calculation of all the eigenvalues is performed using a pseudo-spectral collocation method. This method has been used extensively in the prior literature. The method is based on representing an unknown solution, q, by a Chebyshev partial sum

$$q(y) = \sum_{n=0}^{N} a_n T_n(y), \tag{2.82}$$

where $T_n(y)$ are the Chebyshev polynomials, which can be defined in term of trigonometric function

$$T_n(y) = cos(n \cos^{-1}(y)). \tag{2.83}$$

These polynomials satisfy the orthogonality condition of the form

$$\int_{-1}^{1} \frac{T_n(y)T_m(y)}{\sqrt{1-y^2}} dy = C_n \delta_{nm}, \tag{2.84}$$

with $C_0 = \pi$, $C_n = \frac{\pi}{2}$, $(n \neq 0)$. The discrete Chebyshev expansion coefficients, a_k, are given by

$$a_k = \frac{2}{N c_k} \sum_{j=0}^{N} \frac{q(y_j)\cos(\pi j k)}{c_j}, \quad k = 0, .., N, \qquad c_j = \begin{cases} 2 & j = 0, N, \\ 1 & \text{otherwise}, \end{cases} \tag{2.85}$$

and are evaluated at the extrema of the N-th Chebyshev polynomials given as

$$y_j = \cos(\frac{j\pi}{N}), \quad j = 0, .., N. \tag{2.86}$$

These points are often labelled the Chebyshev Gauss-Lobatto points, a name which alludes to the points role in certain quadrature formulae. When discretizing the stability differential equation, derivatives of the solution are needed as well. These derivatives are approximated by using the derivatives of the interpolating polynomial at these collocation points. The first derivative, for example, is defined by

$$q'(y) = \sum_{n=0}^{N} a_n^{(1)} T_n(y). \tag{2.87}$$

Since $a_{N+1}^{(1)} = 0$ and $a_N^{(1)} = 0$, the non-zero derivative coefficients can be computed in decreasing order by this relation

$$c_k a_k^{(1)} = a_{k+2}^{(1)} + 2(k+1)a_{k+1}, \quad k = N-1, .., 0. \tag{2.88}$$

The interpolating polynomial and its derivatives can also be computed in physical space using multiplication. For more details, we refer to [15]. Upon substitution into the differential equation (2.26) we get

$$F(y,c) \sum_{n=0}^{N} a_n^{(2)} T_n(y) - F'(y,c) \sum_{n=0}^{N} a_n^{(1)} T_n(y) - \alpha^2 F(y,c) \sum_{n=0}^{N} a_n T_n(y) = 0. \tag{2.89}$$

We then require this equation to be satisfied at the Gauss-Lobatto collocations points. This allows us to use the recurrence relation (2.88) or the matrix multiplication in [15] to evaluate the derivatives of the Chebyshev polynomials to get the following equation

$$A_0 q + c A_1 q + c^2 A_2 q = 0, \tag{2.90}$$

where

$$A_0 = -\alpha^2 (E S_j - U_j^2) D_0 q - (E S_j' - 2 U_j U_j') D_1 q + (E S_j - U_j^2) D_2 q, \tag{2.91}$$

$$A_1 = -2\alpha^2 D_0 q - 2 U_j' D_1 q + 2 U_j D_2 q, \qquad A_2 = \alpha^2 D_0 q - D_2 q, \tag{2.92}$$

and

$$\begin{aligned} D_0 q &= \sum_{n=0}^{N} a_n T_n(y_j), \qquad D_1 q = \sum_{n=0}^{N} a_n^{(1)} T_n(y_j), \\ D_2 q &= \sum_{n=0}^{N} a_n^{(2)} T_n(y_j). \end{aligned} \tag{2.93}$$

$D_0, D_1, and D_2$ are known as the differentiation matrices.
The discretized boundary conditions can be written as

$$\sum_{k=0}^{N} a_k T_k(-1) = 0, \qquad \sum_{k=0}^{N} a_k T_k(1) = 0, \tag{2.94}$$

for the case of the free surface boundary conditions case and as

$$\sum_{k=0}^{N} a_k T_k'(-1) = 0, \qquad \sum_{k=0}^{N} a_k T_k'(1) = 0, \tag{2.95}$$

for the wall boundary conditions.

The final result is a generalized eigenvalue problem of the form

$$A a = c B a \tag{2.96}$$

Where the $(2N + 2)$ components vector a and the $(2N + 2) \times (2N + 2)$ matrices A and B are given by

$$a = (\ a_0, a_1, a_2....., a_{N+1}, ca_0, ca_1, ca_2....., ca_{N+1}\ )^T \tag{2.97}$$

$$A = \begin{pmatrix} 0 & I \\ A_0 & A_1 \end{pmatrix}, B = \begin{pmatrix} I & 0 \\ 0 & -A_2 \end{pmatrix} \tag{2.98}$$

The eigenvalues are found using matlab's eig routine which uses the QZ algorithm of LAPACK. In some of the calculation, we have needed A and B to be 1200 x 1200 in order to resolve the unstable modes. Some particular values require higher resolution, but we are limited by computer memory.

2.9 Conclusion

The governing equations of the upper convected Maxwell fluid are presented. A linear stability analysis was applied and the stability equation for the disturbances is derived and then solved analytically for the eigenfunctions. The asymptotic behaviors of the modal solutions of the initial value problem are discussed in order to study the stability of simple parallel shear flows specifically the plane Couette and the plane Poiseuille flows in the limit of infinite Weissenberg and Reynolds numbers.

We found that in the inviscid, nonelastic case all the flows with free surfaces are unstable in the long wave limit. Unlike the plane Couette flow which has no short wave instability, the plane Poiseuille flow has two unstable eigenmodes.

We also described all the details of the numerical method that will be useful to solve efficiently the eigenvalue problem and study the stability of the viscoelastic shear flows in the limit of infinite Weissenberg and Reynolds numbers.

Chapter 3

Stability of plane viscoelastic shear flows in the limit of infinite Weissenberg and Reynolds numbers

3.1 Introduction

In this chapter we address the linear stability of shear flows in the limit of infinite Weissenberg and Reynolds numbers. We consider the viscoelastic upper convected Maxwell model, and we study the stability of few types of shear flows. Most of these flows are unstable for non-elastic inviscid fluids. The effect of elasticity will turn out to always be stabilizing, something which would not be true for flows with curved streamlines. We derive the analytical solutions of the perturbation equation in the long wave limit and we discuss the numerical results obtained by using the Chebyshev collocation method.

3.2 Stability in the long wave limit

We consider the stability problem in the long wave limit, both for the free surface and wall boundary condition. We shall derive sufficient criteria for long wave instability and the resulting algebraic equations are then solved for a few classes of parallel shear flows.
In the long wave limit, the stability equation can be written as

$$F(y,c)q''(y) - F'q' = 0, \tag{3.1}$$

with the boundary condition

$$q(-1) = q(1) = 0 \tag{3.2}$$

for free surfaces.
Here $F(y,c)$ is given by

$$F(y,c) = ES(y) - (U(y) - c)^2. \tag{3.3}$$

This equation (3.1) has the solution $q' = F$, if we have free surface boundary conditions (3.2), we obtain the eigenvalue relation

$$\int_{-1}^{1} F(y,c)dy = 0. \tag{3.4}$$

The roots of this equations are non-real if and only if

$$\int_{-1}^{1} ES(y) - U(y)^2 dy + (\int_{0}^{L} U(y)dy)^2 < 0. \tag{3.5}$$

This inequality shows that unstable eigenvalues cannot exist if ES is sufficiently large.
In the Newtonian case $E = 0$, the Cauchy inequality implies

$$(\int_{-1}^{1} U(y)dy)^2 \leq \int_{0}^{L} U(y)^2 dy, \tag{3.6}$$

with equality only if U is constant. Hence all non-constant velocity profiles satisfy the inequality (3.5), therefore they are unstable.
The case of wall boundary conditions is slight more complicated. If we set $\alpha = 0$ in equation

(2.26), we obtain the solution $q = const.$, which just reflects the undetermined constant in the pressure. Instead of considering the equation (2.26), we set

$$q'(y) = F(y, c)\varphi(y). \tag{3.7}$$

Upon substitution of (3.7) and its derivative into the equation (2.26), we get

$$F\varphi' - \alpha^2 q = 0. \tag{3.8}$$

Differentiating this equation and substituting (3.7) into it, we find

$$(F\varphi')' - \alpha^2 F\varphi = 0. \tag{3.9}$$

When $\alpha = 0$, we find

$$\varphi' = cF^{-1}, \tag{3.10}$$

and the wall boundary conditions provide the relation

$$\int_{-1}^{1} F^{-1}(y, c)dy = 0. \tag{3.11}$$

For the Newtonian case $E = 0$, this can be written as

$$\int_{-1}^{1} \frac{1}{(U - c)^2} dy = 0, \tag{3.12}$$

which is the result found by Heisenberg [5].

Note that the criteria derived here give a necessary and sufficient condition for instability in the limit as $\alpha \to 0$ with a nonzero limit of c_i. There may be instances where the limit of c is real for $\alpha = 0$, but c becomes non-real for small α. In that sense, the criteria derived here are sufficient for long wave instability, but not necessary.

Now that we have derived these criteria for the long wave instability, we will compute the eigenvalues for a few simple base flows, particularly plane Poiseuille and Couette flows, the shear layer and the Bickley jet flows.

3.2.1 Plane Couette and Poiseuille flows

As examples of bounded flows we consider the Couette and Poiseuille flows where the velocity profiles are given by $U(y) = y$ and $U(y) = 1 - y^2$ respectively (See Figure 3.1).

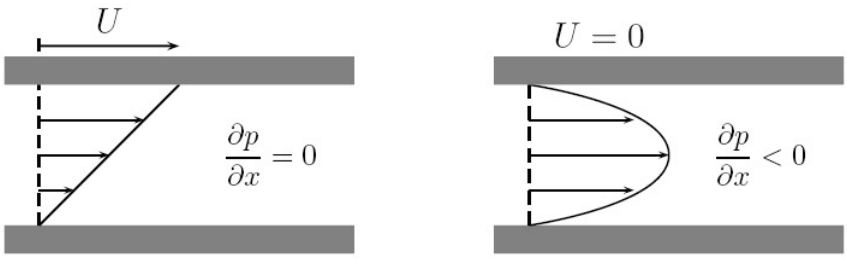

Figure 3.1: Plane Couette and Poiseuille flows.

We will use the above criteria to show the long wave instability both for the free surface boundary condition and for the wall boundary conditions.
Assume further that corresponding normal stress is viscometric, i.e $S(y) = 2U'(y)^2$.
In the case of free surface boundary conditions, the instability criterion is given by

$$\int_{-1}^{1} ES(y) - (U - c)^2 dy = 0. \tag{3.13}$$

For any fixed non-real c, we find

$$\int_{-1}^{1} ES(y) - (U - c)^2 dy = -2c^2 - \frac{2}{3} + 4E, \tag{3.14}$$

and

$$\int_{-1}^{1} ES(y) - (U - c)^2 dy = -2c^2 + \frac{8}{3}c + \frac{16}{3}E - \frac{16}{15} \tag{3.15}$$

respectively, for the Couette flows and the plane Poiseuille and.
The roots of these quadratic equations are real if and only if $E > E_c$, where $E_c = 1/6$ for the Couette flow and $E_c = 1/30$ for the Poiseuille flow.
For the range of elas tic numbers $0 \leq E < E_c$, we encounter two conjugate complex eigenvalues and the flow will be unstable.

If we consider the wall boundary condition, we find

$$\int_{-1}^{1} F(y,c)^{-1}dy = \left\{ \begin{array}{ll} \frac{2}{1-c^2} & E=0 \\ \frac{1}{\sqrt{8E}} \ln \frac{(1+\sqrt{2E}-c)(1+\sqrt{2E}+c)}{(-1+\sqrt{2E}-c)(-1+\sqrt{2E}+c)} & E\neq 0 \end{array} \right\} \tag{3.16}$$

for the plane Couette flow. For the plane Poiseuille flow, we find

$$\int_{-1}^{1} F(y,c)^{-1}dy = -\frac{1}{c(c-1)} + \frac{i}{2(c-1)^{3/2}} \ln \frac{\sqrt{c-1}+i}{\sqrt{c-1}-i}, \tag{3.17}$$

for $E=0$. For $E\neq 0$, we set

$$a = \frac{1}{\sqrt{8E}}, \qquad b = \frac{1-c}{\sqrt{8E}}, \tag{3.18}$$

which leads to the result

$$\begin{aligned} \int_{-1}^{1} F(y,c)^{-1}dy &= \frac{4a^3}{\sqrt{1+4ab}}\Big(\frac{\mathrm{ArTanh}(\frac{2a}{1+\sqrt{1+4ab}})}{1+\sqrt{1+4ab}} \\ &\quad -\frac{\mathrm{ArTanh}(\frac{2a}{1-\sqrt{1+4ab}})}{1-\sqrt{1+4ab}}\Big). \end{aligned} \tag{3.19}$$

For any value of E, we note that no instabilities were found for both plane Poiseuille and Couette flows since there is no non-real eigenvalue c for which the integral equals zero.

3.2.2 Shear layer and Bickley jet flows

In this subsection we consider flows with inflectional profiles, particularly the shear layer flow and the Bickley jet flow which have the velocity profiles $U(y) = \tanh(py)$ and $U(y) = \mathrm{sech}^2(py)$ respectively, with not too small parameter p (see Figure 3.2).

Similarly, as we did for the plane Poiseuille and Couette flows, if we apply the long wave instability criteria for these profiles both for the free surface and the wall boundary conditions, we will obtain algebraic equations that we have to solve for c.
In the free surface boundary condition case, we obtain quadratic equations in the form

$$ac^2 + bc + \gamma = 0 \tag{3.20}$$

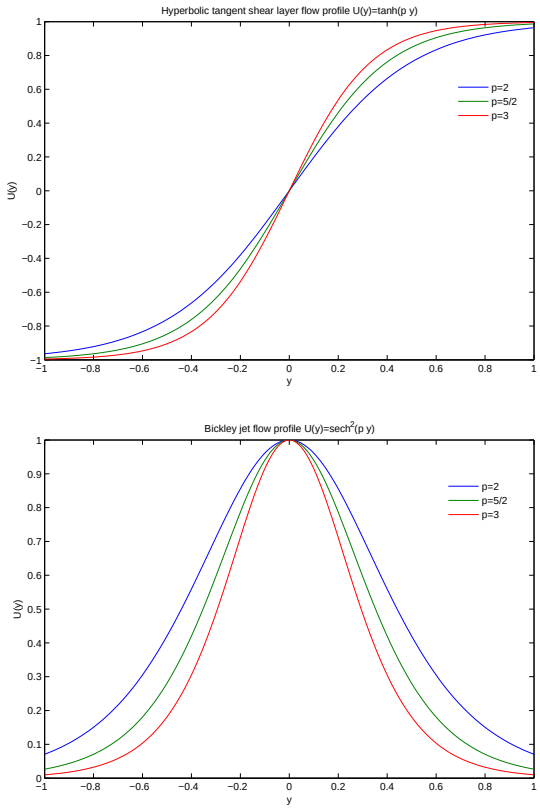

Figure 3.2: Shear layer and Bickley jet flows profiles for $p = 2$, $p = 5/2$, and $p = 3$

where

$$\begin{aligned} a &= -2, \quad b = 0, \\ \gamma &= -2 + \frac{2\tanh(p)}{p} + \frac{8ep}{3}\tanh(p) + \frac{4ep}{3}\mathrm{sech}^2(p)\tanh(p), \end{aligned} \tag{3.21}$$

for the shear layer flow and

$$\begin{aligned} a &= -2, \quad b = \frac{4\tanh(p)}{p}, \\ \gamma &= \frac{2(8Ep^2+1)\tanh(p)^3}{3p} - \frac{16Ep\tanh(p)^5}{5} - \frac{2\tanh(p)}{p}, \end{aligned} \tag{3.22}$$

for the Bickley jet flow.

The case of wall boundary conditions is slightly more complicated, we find algebraic equations in the form

$$G(c, E, p) = 0 \tag{3.23}$$

where

$$G(c, E, p) = \int_{\tanh(-p)}^{\tanh(p)} (p(1-t^2)(2Ep^2(1-t^2)^2 - (t-c)^2)^{-1} dt \tag{3.24}$$

for the shear layer flow and

$$G(c, E, p) = \int_{\tanh(-p)}^{\tanh(p)} (p(1-t^2)(8Ep^2t^2(1-t^2)^2 - (1-c-t^2)^2))^{-1} dt \tag{3.25}$$

for the Bickley jet flow.

These equations are solved numerically for c by using Newton's Method at different values of the parameters p and E. Newton iteration proceeds by linearizing the equation at each iterate:

$$G(c_n, E, p) + DG(c_n, E, p)(c_{n+1} - c_n) = 0$$

Here DG denotes the Jacobian matrix with entries $\partial G_i \partial_j$. The advantage of Newton's iteration is that it is guaranteed to converge rapidly if the initial guess is close enough to the solution. The disadvantage is that it requires the evaluation and inversion of the Jacobian.

3.3 Stability results

In this section we present and discuss the temporal stability characteristics of the various profiles. The numerical computations were done using the Chebyshev collocation spectral method, which is widely used in the literature. For specifics of the method, we refer to [15]. We consider flows bounded by free surfaces as well flows bounded by walls. In the results reported below, the number of Chebyshev modes used in the computation varies. We carefully checked that we used a sufficient number of modes to obtain converged results. In some of our calculations we choose N to be equal 600 to resolve the unstable modes.

We can conclude some general trends from the analytical results given above. The Howard semicircle theorem guarantees that there are no unstable eigenvalues if E is sufficiently large, provided S has a lower bound. Even in flows where there is a point where $S = 0$, we see this stabilization by elasticity. On the other hand, unbounded flows where $S \to 0$ at infinity have been found not to be fully stabilized [2, 9].

In the broader context of viscoelastic flow, we can interpret inviscid instabilities as a resonant interaction between forward and backward traveling waves. For such an interaction to occur, the range of fluid speeds must cover at least twice the elastic wave speed. If E is large, the elastic wave speed is large, and no resonant interaction is possible. On the other hand, the wave speed is zero if $E = 0$. In this case, all nonuniform flows are unstable to long waves for the free surface boundary condition. On the other hand, the stability of wall bounded flows is a quite complicated problem.

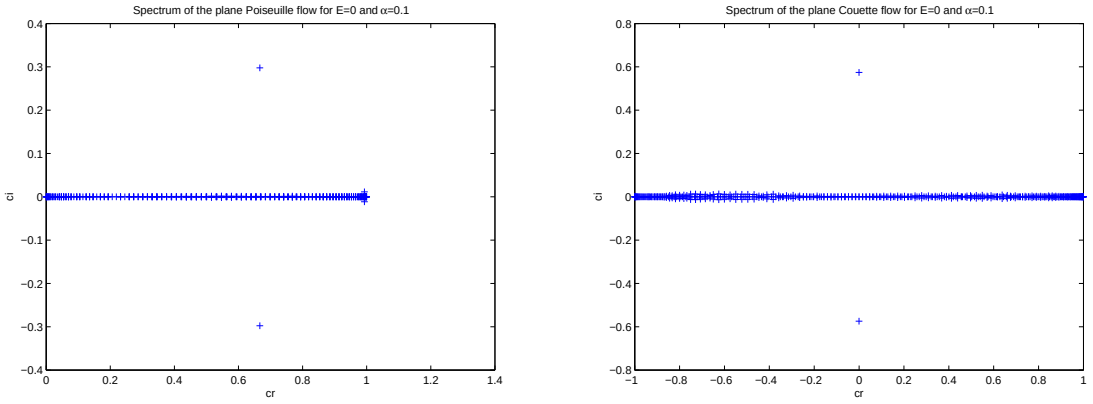

Figure 3.3: Eigenspectrum for the (PPF) flow, $U(y) = 1-y^2$, and the (PCF) flow, $U(y) = y$, using the free surface boundary condition

In Figures 3.5 and 3.4, we show the computed eigenspectra for plane Poiseuille flow (PPF) and plane Couette Flow (PCF) in the inviscid case $E = 0$. For the free surface boundary condition we encounter complex conjugate eigenvalues, as expected from the long wave analysis. In agreement with well known theory, no instabilities were found by setting the wall boundary condition (see Figure 3.4).
For the hyperbolic tangent shear layer and the Bickley jet flows, both types of boundary conditions lead to instability for not too small values of the parameter p.

The effect of the elasticity number E is shown in Figures 3.7 and 3.8. In both Couette and Poiseuille flow, elasticity stabilizes the inviscid instability of the free surface flow. For high

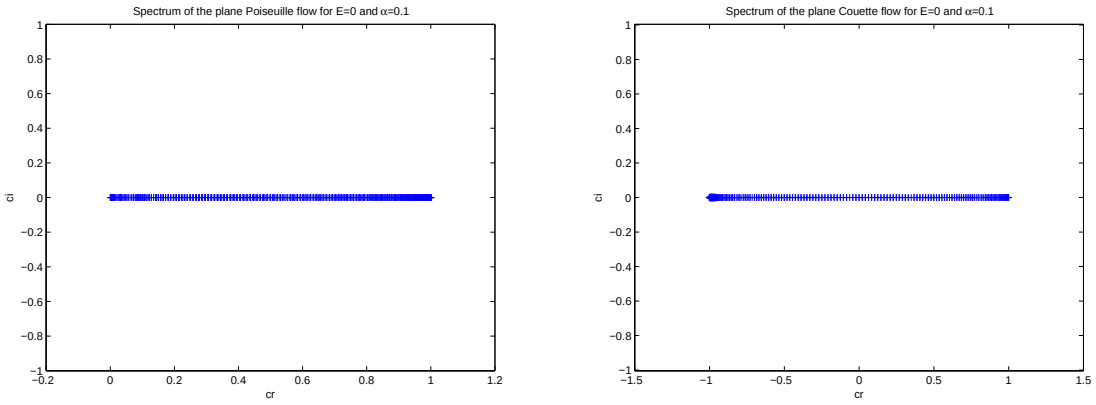

Figure 3.4: Eigenspectrum for the (PPF) flow, $U(y) = 1 - y^2$, and the (PCF) flow, $U(y) = y$, using the wall boundary condition

enough elasticity, the flow becomes completely stable. We note that, in the case of Poiseuille flow, long waves are stabilized before the flow is completely stabilized. Another noteworthy feature is the presence of a short wave instability in the inviscid plane Poiseuille flow between two free surfaces. We have verified using asymptotic methods that indeed the imaginary part of c does not reach zero at a finite α, but tends to zero as $1/\alpha^2$. The associated eigenfunction becomes localized near the free surface. To our knowledge, no such feature has ever been found in wall bounded shear flows. A detailed analysis will be given in the chapter 4.

The hyperbolic tangent shear layer and Bickley jet flows also show generally similar trends. We consider the cases of $p = 2$, $p = 5/2$ and $p = 3$ for both flows as representative cases, for free surface and wall boundary conditions. These results are displayed in Figures 3.9-3.12. The plots show the imaginary part of the most unstable eigenvalue. We have found that an increase of the elasticity number has a stabilizing effect on these flows and the value of the imaginary part of the eigenvalue increases as we increase the parameter p.

We also note the absence of the short wave instability when the wavenumber α exceeds a critical value, which increases with the parameter p. This means no short wave instabilities were found for the shear and the Bickley jet flows by using either the free surface or the wall boundary conditions. This is also the case for the plane Couette flow, but not for the plane Poiseuille flow which has short wave instability when we consider the free surface boundary

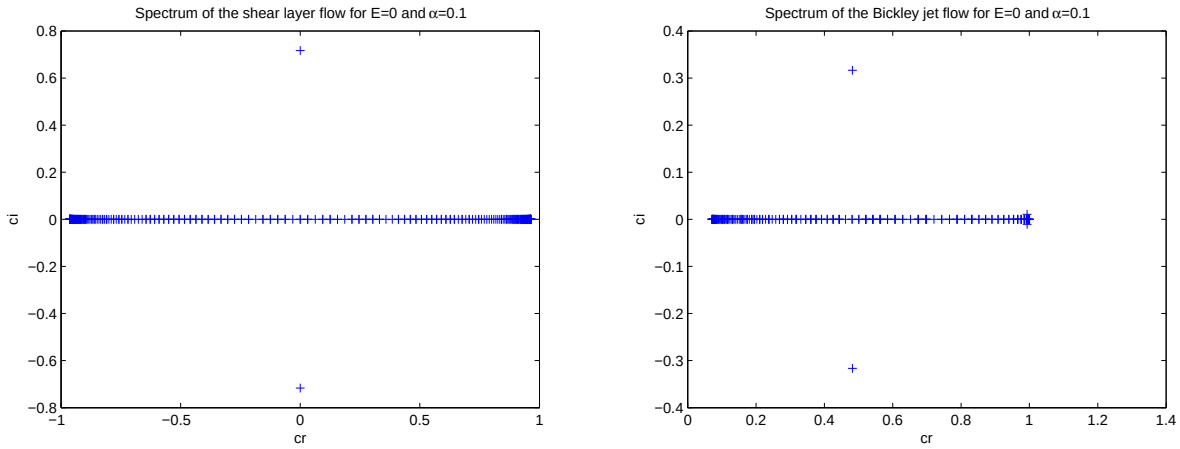

Figure 3.5: Eigenspectrum for the shear layer flow, $U(y) = \tanh(2y)$, and the Bickley jet flow, $U(y) = \mathrm{sech}^2(2y)$, using the free surface boundary condition

conditions.

For the Bickley jet, this is actually a composite plot of two different eigenvalues. Figure 3.13 shows the imaginary parts of both eigenvalues. The symmetry of the eigenfunction for the two eigenvalues is opposite: The long wave instability ("Eigenvalue 2" in the plot) is due to a symmetric (varicose) mode, while the other eigenvalue belongs to an antisymmetric (sinuous) mode. In the inviscid case $E = 0$, the transition between the modes shifts to very small values of α. We can get some partial insight into this behavior by comparing with the unbounded Bickley jet. In the unbounded Bickley jet, the most unstable mode is sinuous, see [3] (we note that the designation as "even" in [3] refers to the parity of the streamfunction). The long wave instability in the wall bounded case, however, is varicose. As the wave number increases, the instability shifts from this varicose long wave mode to the sinuous mode that we would expect from the results on the unbounded case. For free surface boundary conditions, on the other hand, the long wave mode is sinuous. An asymptotic analysis elucidating the transition from the bounded to the unbounded Bickley jet would be a meritorious undertaking for future research. We found nothing on this in the literature; indeed there seems to be very little work on the bounded Bickley jet.

The results for the wall bounded shear layer show that elasticity is not always uniformly

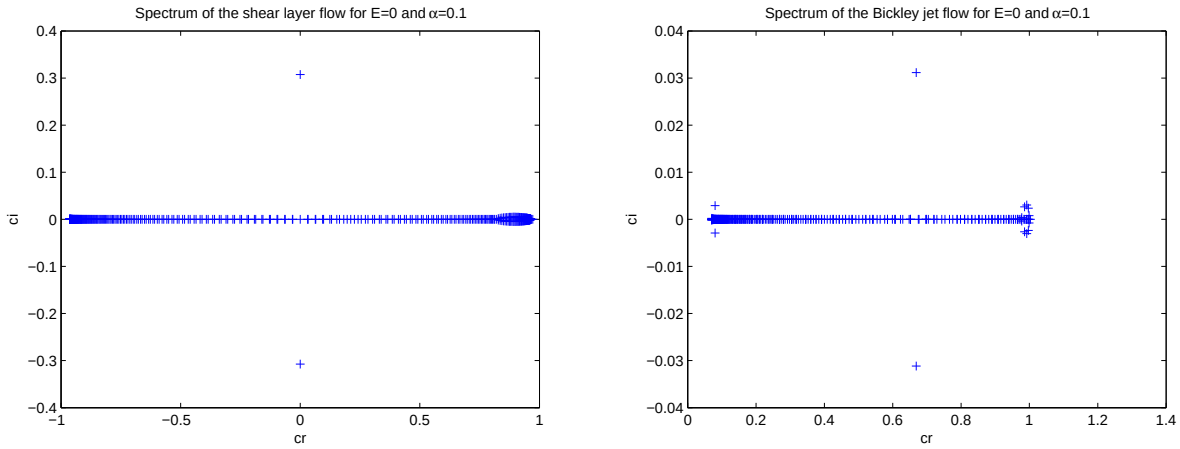

Figure 3.6: Eigenspectrum for the shear layer flow, $U(y) = \tanh(2y)$, and the Bickley jet flow, $U(y) = \mathrm{sech}^2(2y)$, using the wall boundary condition

stabilizing; a small amount of elasticity actually destabilizes long waves. We can give a heuristic explanation of this by considering the limit for small E. If we set $c = c_0 + Ec_1 + ...$, we obtain

$$c_1 = \frac{\int_{-1}^{1}(U(y) - c_0)^4 S(y)\, dy}{2\int_{-1}^{1}(U - c_0)^3\, dy}. \tag{3.26}$$

In the inviscid case, $c_0 = i\gamma$ is purely imaginary. The imaginary part of $(U - c_0)^3$ is $-3U^2\gamma + \gamma^3$. If p is moderately large, we have $U = \pm 1$ over must of the the interval, and therefore the sign of $-3U^2\gamma + \gamma^3$ will be opposite to that of γ. On the other hand, S is concentrated near the centerline where $U = 0$, so we expect the integral in the numerator to be positive. As a consequence, at least for large p, the imaginary part of c_1 will have the same sign as γ, i.e. the inviscid long wave instability is enhanced by a small amount of elasticity.

We compared our numerical results with the analysis of the long wave limit above and found excellent agreement. We show the results for the all types of flows. The comparison is shown in Tables 3.1- 3.8.

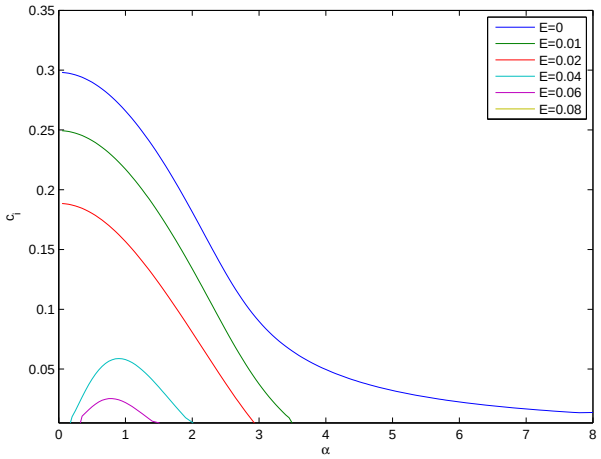

Figure 3.7: Effect of the elasticity number on the plane Poiseuille Flow (PPF), $U(y) = 1-y^2$, using the free surface boundary condition

3.4 Conclusion

The effect of elasticity on the linear stability of several shear flow profiles has been studied using the Chebyshev collocation spectral method. In the inviscid, nonelastic case all profiles are unstable for free surface boundary conditions. In the case of wall bounded flow, there are instabilities in the shear layer and Bickley jet flows. In all cases, elasticity has a stabilizing effect.

Stability in the long wave limit can be determined analytically. The results were compared to the numerical solutions and excellent agreement is shown. Unlike the inviscid case, we found flows which are long wave stable, but nevertheless unstable to wave numbers in a certain finite range. While elasticity is ultimately stabilizing, this effect is not monotone; there are instances where a small amount of elasticity actually destabilizes the flow. Linear stability in the short wave limit of the inviscid plane Poiseuille flow will be investigated in the next chapter.

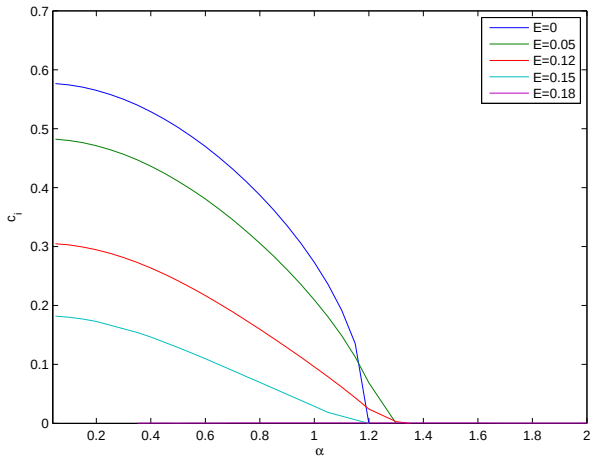

Figure 3.8: Effect of the elasticity number on the plane Couette Flow (PCF), $U(y) = y$, using the free surface boundary condition

Table 3.1: Eigenvalues in the plane Poiseuille flow ($U(y) = 1 - y^2$, as a function of elasticity number for free surface conditions.

E	**c** (numerical)	**c** (analytic)
0	0.666667 + 0.298142i	0.666667 + 0.298142i
0.01	0.666667 + 0.249444i	0.666667+ 0.249443i
0.02	0.666667+ 0.188561i	0.666667 + 0.188561i
0.06	1.000081	1.000000
0.12	1.000003	0.999982

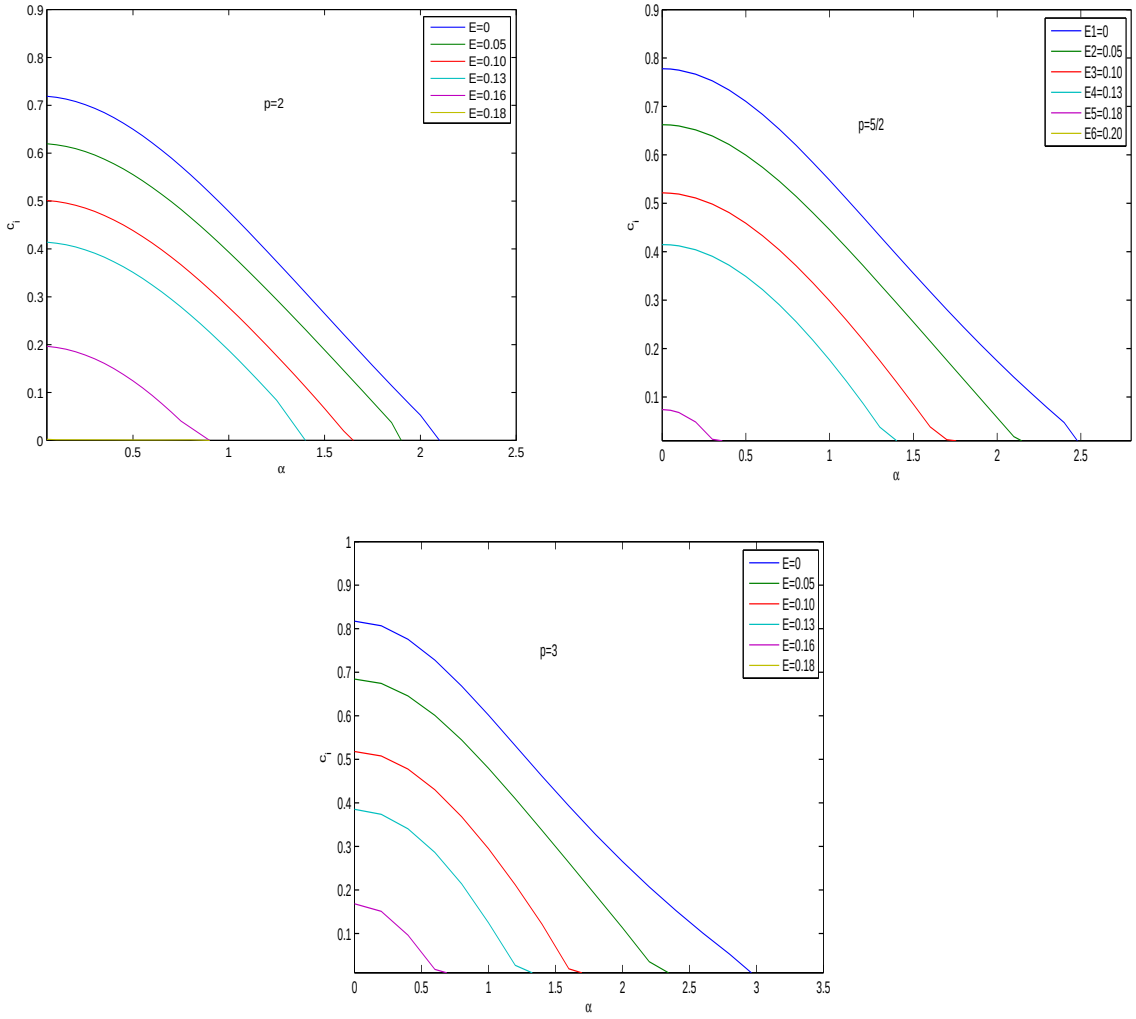

Figure 3.9: Effect of the elasticity number on the hyperbolic tangent shear layer flow, $U(y) = \tanh(py), p = 2, p = 5/2, and p = 3$, using the free surface boundary. condition.

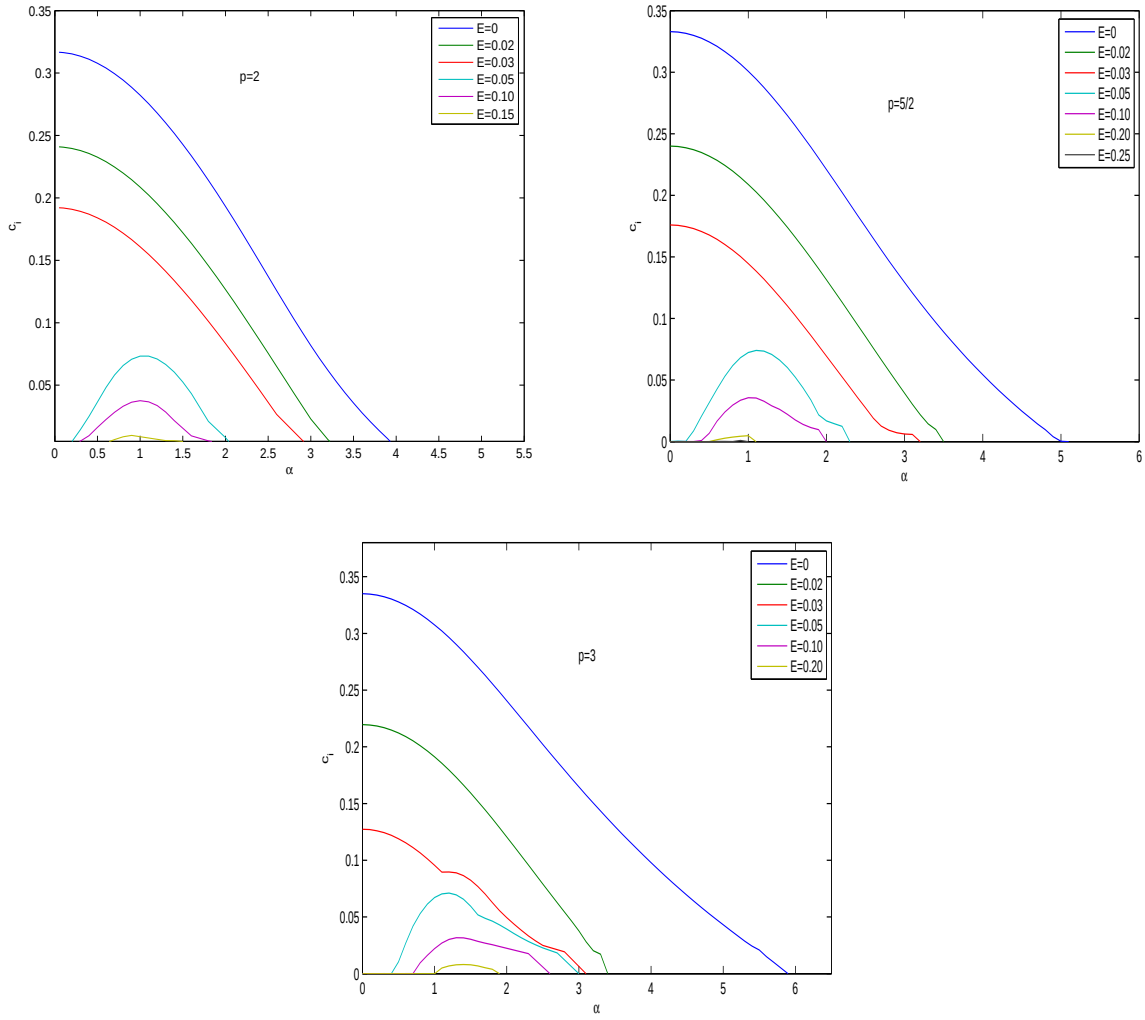

Figure 3.10: Effect of the elasticity number on the Bickley jet flow, $U(y) = \mathrm{sech}^2(py), p = 2, p = 5/2, and p = 3$, using the free surface boundary condition.

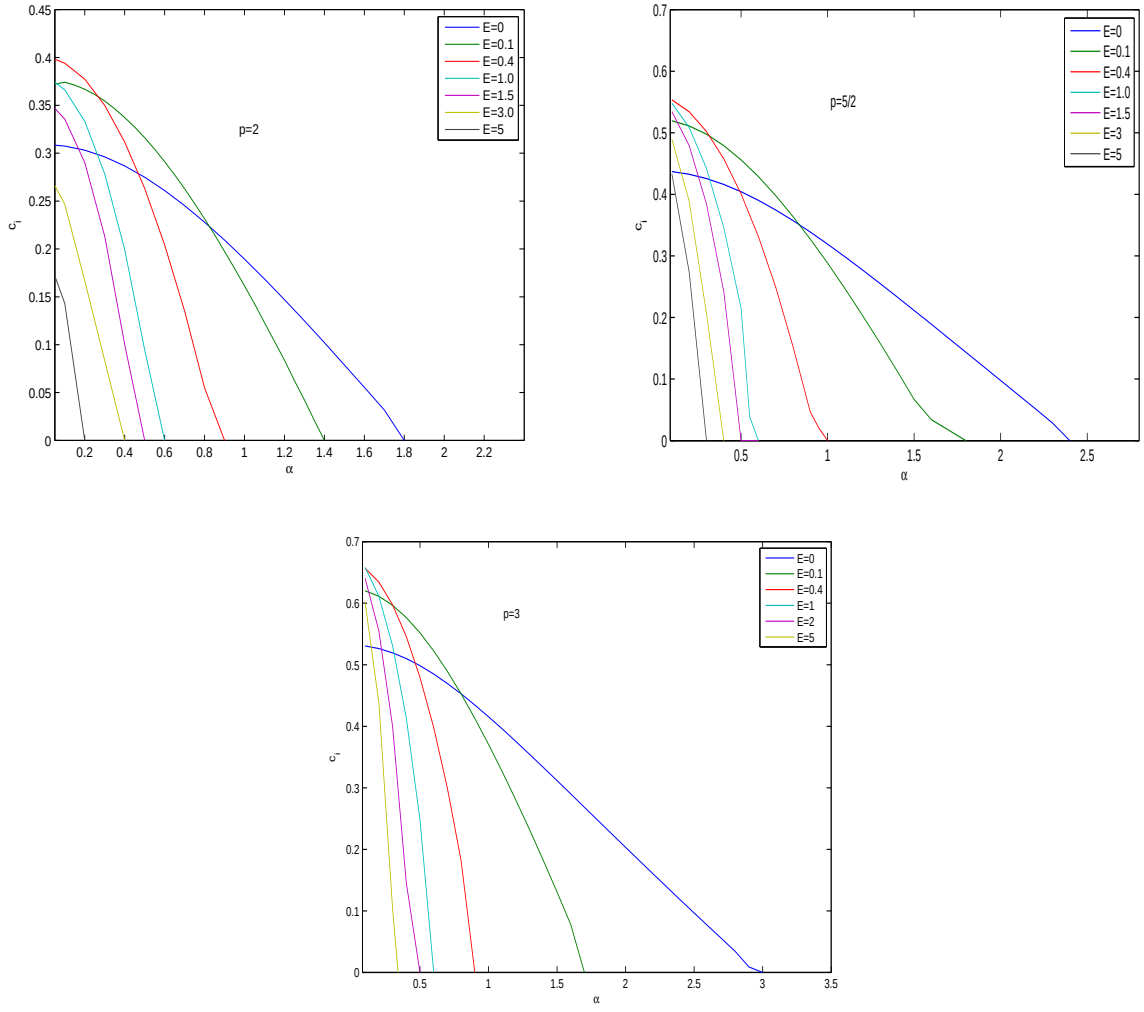

Figure 3.11: Effect of the elasticity number on the hyperbolic tangent shear layer flow, $U(y) = \tanh(py), p = 2, p = 5/2, and p = 3$, using the wall boundary condition.

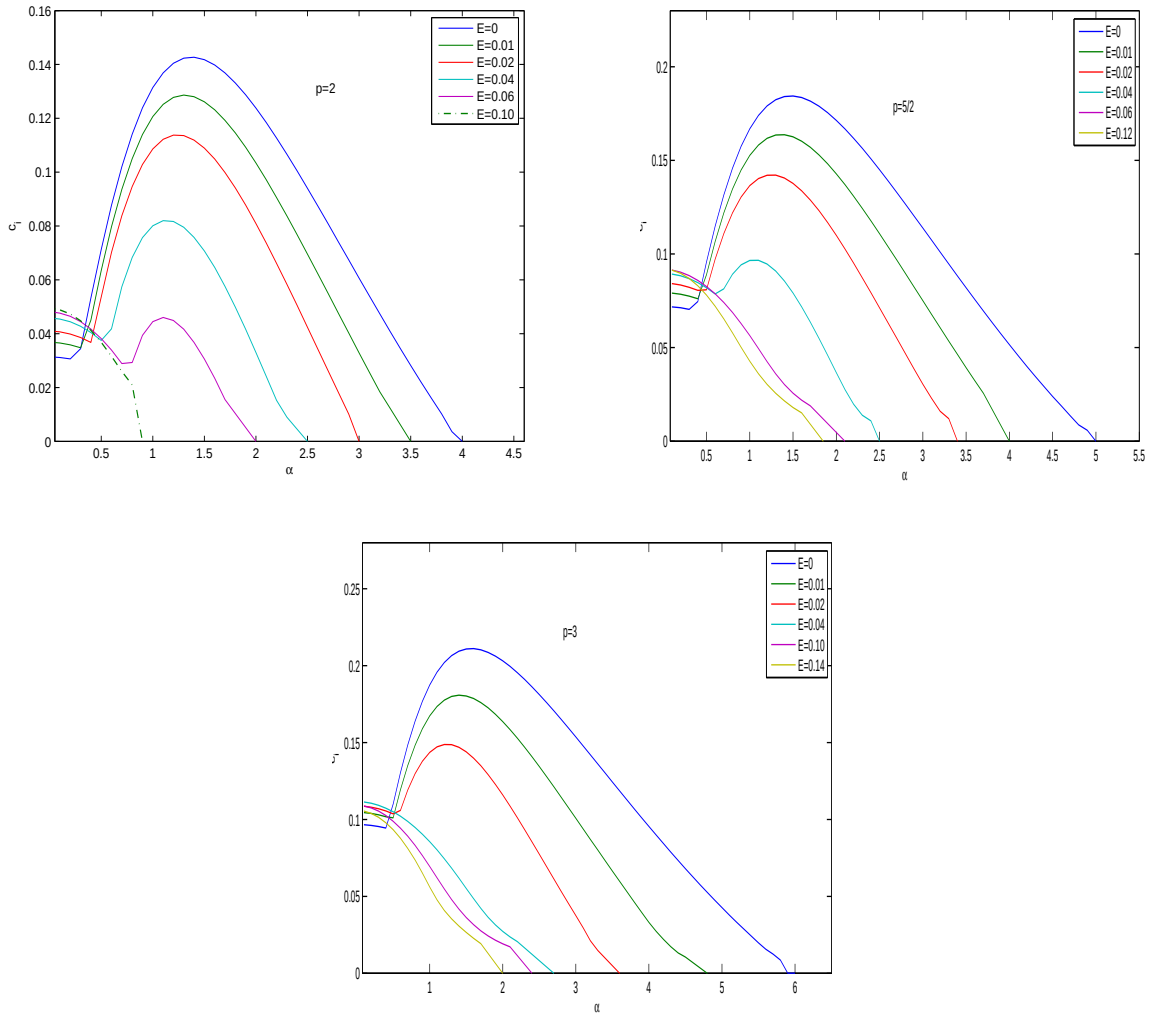

Figure 3.12: Effect of the elasticity number on the Bickley jet flow, $U(y) = \mathrm{sech}^2(py), p = 2, p = 5/2, and p = 3$, using the wall boundary condition.

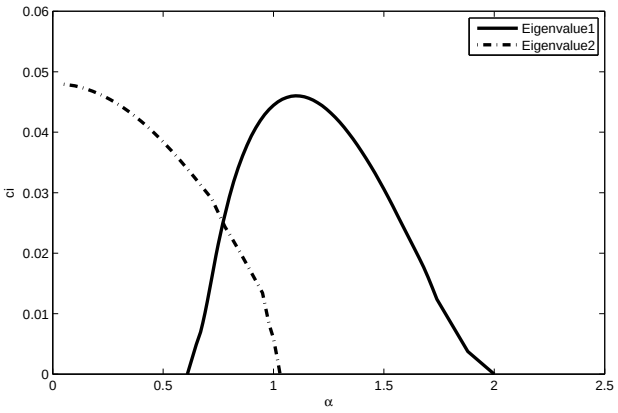

Figure 3.13: Eigenvalues for Bickley jet flow, $U(y) = \mathrm{sech}^2(2y)$, using the wall boundary condition, E=0.06.

Table 3.2: Eigenvalues in the Couette flow ($U(y) = y$, as a function of elasticity number for the free surface boundary conditions.

E	**c** (numerical)	**c** (analytic)
0	0.577348i	0.577348i
0.05	0.483044021905644i	0.483044026615014i
0.12	0.305503322292285i	0.305503329672230i
0.15	0.182572635416244i	0.182572675534330i
0.18	0	0

Table 3.3: Eigenvalues (for $\alpha \to 0$) in the shear layer flow ($U(y) = \tanh(py), p = 2$), as a function of elasticity number both for free surface and wall boundary conditions.

Free surface			Wall		
E	**c** (numerical)	**c** (analytic)	E	**c** (numerical)	**c** (analytic)
0	0.719646 i	0.719712 i	0	0.308876 i	0.308838 i
0.05	0.620348 i	0.620410 i	0.1	0.376918 i	0.376756 i
0.10	0.501768 i	0.501828 i	0.4	0.399554 i	0.399609 i
0.13	0.414650 i	0.414710 i	1	0.376888 i	0.376996 i
0.18	0.197180 i	0.197248 i	1.5	0.350411 i	0.350560 i
			3	0.272332 i	0.272591 i
			5	0.181482 i	0.181497 i

Table 3.4: Eigenvalues (for $\alpha \to 0$) in the shear layer flow ($U(y) = \tanh(py), p = 5/2$), as a function of elasticity number both for free surface and wall boundary conditions.

Free surface			Wall		
E	**c** (numerical)	**c** (analytic)	E	**c** (numerical)	**c** (analytic)
0	0.778043i	0.778043i	0	0.437425i	0.4379696i
0.05	0.662367i	0.662367i	0.1	0.520826i	0.521473i
0.10	0.521640i	0.521640i	0.4	0.559866i	0.558255i
0.13	0.414892i	0.414892i	1	0.561083i	0.561084i
0.18	0.074258i	0.074258i	1.5	0.552538i	0.552538i
			3	0.521658i	0.521658i
			5	0.482755i	0.482755i
			5	0.447771i	0.447771i

Table 3.5: Eigenvalues (for $\alpha \to 0$) in the shear layer flow ($U(y) = \tanh(py), p = 3$), as a function of elasticity number both for free surface and wall boundary conditions.

Free surface			Wall		
E	**c** (numerical)	**c** (analytic)	E	**c** (numerical)	**c** (analytic)
0	0.817504 i	0.817504 i	0	0.531755304642808i	0.531784744101468i
0.05	0.684334 i	0.684339 i	0.1	0.622667770167579i	0.624320228490253i
0.10	0.518004 i	0.518003 i	0.4	0.663551905400277i	0.663551918534356i
0.13	0.385140 i	0.385139 i	1	0.672534323120355i	0.672534281654398i
0.16	0.168338 i	0.168338 i	2	0.666690292290481i	0.666690292185758i
			5	0.639400231535711i	0.639400232609013i
			7	0.622783473280798i	0.622783481386810i

Table 3.6: Eigenvalues (for $\alpha \to 0$) in the Bickley jet flow ($U(y) = \mathrm{sech}^2(py), p = 2$), as a function of elasticity number both for free surface and wall boundary conditions.

Free surface			Wall		
E	**c** (numerical)	**c** (analytic)	E	**c** (numerical)	**c** (analytic)
0	0.482014+0.316790i	0.482014+0.316791i	0	0.669015+0.031275i	0.669022+0.031328i
0.02	0.482014+0.240997i	0.482014+0.240998i	0.01	0.687757+0.036747i	0.687760+0.036758i
0.03	0.482014+0.192201i	0.482014+0.192202i	0.04	0.715255+0.045686i	0.715172+0.045740i
0.05	0.408699; 0.555090	0.4089700; 0.555058	0.06	0.725872+0.047709i	0.725882+0.048022i
0.10	0.1487946; 0.815222	0.148806; 0.815222	0.1	0.740284+0.049222i	0.740886+0.049338i

Table 3.7: Eigenvalues (for $\alpha \to 0$) in the Bickley jet flow ($U(y) = \mathrm{sech}^2(py), p = 5/2$), as a function of elasticity number both for free surface and wall boundary conditions.

Free surface			Wall		
E	**c** (numerical)	**c** (analytic)	E	**c** (numerical)	**c** (analytic)
0	0.394656+0.332920i	0.394656+0.332920i	0	0.688206+0.071923 i	0.688206+0.071923 i
0.01	0.394655+0.290183i	0.394655+0.290183i	0.01	0.717482+0.079338i	0.717480+0.079337i
0.02	0.394653+0.239952i	0.394653+0.239952i	0.02	0.734653+0.084395i	0.734647+0.084395i
0.03	0.394650+0.175920i	0.394650+0.175920i	0.04	0.756512+0.089545i	0.756476+0.089575i
			0.06	0.771020+0.091588i	0.771020+0.091738i
			0.12	0.798639+0.091809i	0.797803+0.092324i
			0.15	0.814328+0.090134i	0.817962+0.089234i

Table 3.8: Eigenvalues (for $\alpha \to 0$) in the Bickley jet flow ($U(y) = \mathrm{sech}^2(py), p = 3$), as a function of elasticity number both for free surface and wall boundary conditions.

Free surface			Wall		
E	**c** (numerical)	**c** (analytic)	E	**c** (numerical)	**c** (analytic)
0	0.394646+0.332941i	0.394646+0.332941i	0	0.713317+0.096673i	0.713317+0.096673i
0.05	0.394646+0.239972i	0.394646+0.239972i	0.01	0.753586+0.104616i	0.753585+0.104618i
0.10	0.394645+0.175940i	0.394645+0.175941i	0.02	0.775578+0.108829i	0.775584+0.108818i
			0.04	0.802454+0.111564i	0.802548+0.111614i
			0.10	0.841570+0.107558i	0.842227+0.109192i
			0.14	0.860138+0.105913i	0.856128+0.105952i

Chapter 4

Surface modes in inviscid free surface shear flows

4.1 Introduction

We investigate the linear stability of inviscid plane Poiseuille flow between two parallel free surfaces. We will show that there are short wave instabilities with eigenfunctions localized near the free surface and derive the asymptotics of these modes. The stability of wall bounded inviscid shear flows has been studied for more than a century. We refer to [3] for a review of the subject. However, shear flows bounded by free surfaces are also a solution of the Euler equations. Although there are entire books on stability of films and jets [18, 25], these studies have focussed on instabilities due to surface effects, such as surface tension and air drag, and they usually assume a uniform velocity within the jet or film. [17] consider an axisymmetric jet bounded by a free surface with a Hagen-Poiseuille profile of the velocity. They conclude that the nonuniform velocity in the jet has a stabilizing effect. This conclusion, however, is due to their failure to consider nonaxisymmetric modes [21].

In recent work by one of the authors in [21], it was shown that plane parallel shear flows bounded by two free surfaces have long wave instabilities for all velocity profiles that are not

uniform. This is in marked contrast to the wall bounded case, where criteria such as those of Rayleigh and Fjørtoft guarantee stability of a broad class of flows.

In this chapter, we shall show that some flows, such as plane Poiseuille flow, also have short wave instabilities. Again, this is in marked contrast to the wall bounded case. In this case, no smooth velocity profiles unstable to short waves are known, and for certain classes of flows there are even results ruling out short wave instability [19, 22].

We consider flow in the strip $-1 < z < 1$, with a base flow profile given by $U(z)$. We prefer to formulate the linear stability problem in terms of the perturbation pressure rather than a stream function. We assume the perturbation pressure is given in the form

$$p(x, z) = \exp(i\alpha(x - ct))q(z). \tag{4.1}$$

The Rayleigh equation for linear stability then takes the form

$$(U(z) - c)(q'' - \alpha^2 q) - 2U'(z)q' = 0. \tag{4.2}$$

For free surfaces, the boundary conditions are $q(-1) = q(1) = 0$.

We shall show below that, for plane Couette flow $U(z) = z$, unstable modes exist only for $\alpha < 1.19968$. In contrast, we shall show that plane Poiseuille flow has unstable modes in the limit $\alpha \to \infty$. The corresponding eigenfunctions are localized at the free surface. This implies that analogous instabilities exist in any shear flow in which the shear rate has a maximum at the free surface. Moreover, the instability will also exist in flows bounded by a wall on one side and a free surface on the other. In such flows, it is known that there are no instabilities in the long wave limit [18, 21].

4.2 The case of Couette flow

In this section, we shall show that plane Couette flow has no short wave instability. For $U(z) = z$, the linear stability equation takes the form

$$(z - c)(q'' - \alpha^2 q) - 2q' = 0. \tag{4.3}$$

The general solution of this equation is

$$\begin{aligned} q(z) = \quad & c_1(\alpha(z-c)\cosh(\alpha(c-z)) + \sinh(\alpha(c-z))) \\ & + c_2(\alpha(z-c)\sinh(\alpha(c-z)) + \cosh(\alpha(c-z))). \end{aligned} \tag{4.4}$$

By inserting this into the boundary conditions, we find the eigenvalue relation

$$c^2 = 1 + \frac{1}{\alpha^2} - \frac{2}{\alpha \tanh 2\alpha}. \tag{4.5}$$

The function on the right hand side is negative for small α, but changes its sign to positive at $\alpha = 1.19968$ and then remains positive. Hence unstable modes exist only for the range values $0 < \alpha < \alpha_c$. In the long wave limit $\alpha \to 0$, the pwer series expansion of the right hand side of (4.5) gives

$$c^2 = -1/3 + \frac{16}{45}\alpha^2 - \frac{128}{945}\alpha^4 + O\left(\alpha^5\right).$$

This implies we encounter two complex conjugate eigenvalue $c = \pm\frac{i}{\sqrt{3}}$ as α goes to zero. Hence the unstable modes exist for the long waves.

In the short wave limit $\alpha \to 0$, the relation leads to real eigenvalues which implies none of the eigenvalues are unstable.

The effect of the elasticity number on the stability of the Couette flow with free surface has been studied in the previous chapter. It is shown that an increase of the elasticity has a stabilizing and the flow remains stable for $\alpha > \alpha_c$ and that the critical value of α_c increases with the elasticity number E.

4.3 Plane Poiseuille flow

In this section, we consider the inviscid instability problem in the short wave limit for plane Poiseuille flow where the velocity profile is given by $U(z) = 1 - z^2$.

The linear stability equation takes this form

$$(1 - c - z^2)(q'' - \alpha^2 q) + 4zq' = 0. \tag{4.6}$$

We impose the boundary conditions

$$q(0) = \lim_{y\to\infty} q(y) = 0. \tag{4.7}$$

It can be seen that the stability equation has a singularity at the pont z_c in the domain of flow where $U(z_c) = c$ if $0 \leq c \leq 1$. It will be shown that critical layers are important in solving the initial value problem.

In the long wave limit, the general solution of the equation (4.7) is given by

$$q(z) = A_1 + B_1(-15 + 30c - 15c^2 + (10 + 40E - 10c)z^2 - 3z^4)z, \tag{4.8}$$

for some constants A_1 and B_1.

By using the free surface boundary conditions, we find the eigenvalue relation

$$\frac{16}{15} - \frac{16}{3}E - \frac{8}{3}c + 2c^2 = 0. \tag{4.9}$$

The roots of this quadratic equation are real if $E > E_c$ where ($E_c = 1/30$). We conclude that in the long wave limit the Poiseuille flow is unstable for the range of elastic numbers $0 < E < E_c$. In newtonian case $E = 0$, we encountered two complex conjugate eigenvalues given by $c = \frac{2}{3} \pm \frac{2\sqrt{5}}{15}i$.

In the short wave limit, we will look for eigenmodes localized near one of the walls, say $z = -1$, and we set $z = -1 + y/\alpha$, $c = s/\alpha$. Our differential equation now becomes

$$(2y - \frac{y^2}{\alpha} - s)(q'' - q) - 4(1 - \frac{y}{\alpha})q' = 0. \tag{4.10}$$

We seek a perturbation series in the form

$$\begin{aligned} q &= q_0 + \frac{q_1}{\alpha} + ..., \\ s &= s_0 + \frac{s_1}{\alpha} + ... \end{aligned} \tag{4.11}$$

On substituting these expressions into the differential equation (4.10), we obtain

$$(-\tfrac{y^2}{\alpha} + 2y - s_0 - \tfrac{s_1}{\alpha})(q_0'' - q_0 + \tfrac{1}{\alpha}(q_1'' - q_1)) + 4(\tfrac{y}{\alpha} - 1)(q_0' + \tfrac{q_1'}{\alpha}) = 0. \tag{4.12}$$

By comparing the terms of $\frac{1}{\alpha}$, we find

$$((2y-s_0)(q_0''-q_0)-4q_0')+\tfrac{1}{\alpha}(-(y^2+s_1)(q_0''-q_0)+(2y-2)(q_1''-q_1)+4(yq_0'-q_1'))$$
$$+\tfrac{1}{\alpha^2}(-(y^2+s_1)(q_1''-q_1)+4yq_1')=0. \tag{4.13}$$

At the leading order, we find the equation

$$(2y-s_0)(q_0''-q_0)-4q_0'=0. \tag{4.14}$$

The solution of this differential equation is given by

$$q_0(y)=C_1(2+s_0-2y)e^y+C_2(-2+s_0-2y)e^{-y}. \tag{4.15}$$

By applying the boundary conditions (4.7), we get
$C_1=0$ and $s_0=2$.
This leads to the closed form solution

$$q_0(y)=ye^{-y}, \qquad s_0=2. \tag{4.16}$$

At the next order, we find the problem

$$(2y-s_0)(q_1''-q_1)-4q_1'=(s_1+y^2)(q_0''-q_0)-4yq_0'. \tag{4.17}$$

Mathematica produces the following particular solution:

$$q_1=-\frac{c_1}{2\alpha}e^{-y}+\frac{1}{4e^2\alpha}(2e^y(y-2)\mathrm{Ei}(2-2y)+e^{2-y}y(1-2y+2\log(y-1))). \tag{4.18}$$

Conventionally, the branch cut for the function Ei is placed on the negative real axis. Given our boundary condition at infinity given by (4.7), we prefer a branch cut on the positive real axis. In the notation of [16], this function is given by $-E_1(-x)$, which agrees with $\mathrm{Ei}(x)$ except for the choice of branch cut. We therefore choose the alternative solution

$$q_1=-\frac{c_1}{2\alpha}e^{-y}+\frac{1}{4e^2\alpha}(-2e^y(y-2)E_1(2y-2)+e^{2-y}y(1-2y+2\log(y-1))). \tag{4.19}$$

This solution already satisfies the condition at infinity. To determine c_1, we need to satisfy $q_1(0)=0$. In imposing this condition, we must take care to choose the correct branch. Note

that the singular point of the differential equation is in the upper half plane if $\mathrm{Im}(s_1) > 0$ and in the lower half plane if $\mathrm{Im}(s_1) < 0$. Correspondingly, we require that

$$\lim_{\epsilon \to 0} q_1(0 - i\epsilon \,\mathrm{sign}(s_1)) = 0. \tag{4.20}$$

The outcome of this calculation is

$$s_1 = -\frac{2}{e^2}\mathrm{Ei}(2) \pm \frac{2\pi i}{e^2}. \tag{4.21}$$

and the eigenvalues are in the form

$$c \sim \frac{2}{\alpha} + \frac{2}{\alpha^2 e^2}(-\mathrm{Ei}(2) \pm \pi i). \tag{4.22}$$

It might appear as though the function $q_1(y)$ has a logarithmic singularity at $y = 1$, but it does not. The logarithmic terms cancel, and the leading nonanalytic contribution is actually or order $(y-1)^3 \log(y-1)$. This is linked to the fact that the roots of the indicial equation for the regular singular point, where $U(z) = c$, are 3 and 0, regardless of the value of c. As a consequence, the approximation $q_0 + q_1/\alpha$ for the eigenfunction is uniformly valid, even near the singular point.

4.4 Numerical results

We solved the eigenvalue problem for plane Poiseuille flow numerically using a Chebyshev discretization. The imaginary part of the eigenvalues as function of $log(\alpha)$ is shown in Figure (4.1). Table 4.1 compares our numerical eigenvalues against the predictions of the formula

$$c \sim \frac{2}{\alpha} + \frac{2}{\alpha^2 e^2}(-\mathrm{Ei}(2) \pm \pi i). \tag{4.23}$$

There are two eigenmodes corresponding to the two free surfaces at $z = \pm 1$. The two eigenmodes can be combined into an even and an odd eigenfunction. The difference between the two eigenvalues tends to zero exponentially with α as shown in Figure (4.2).

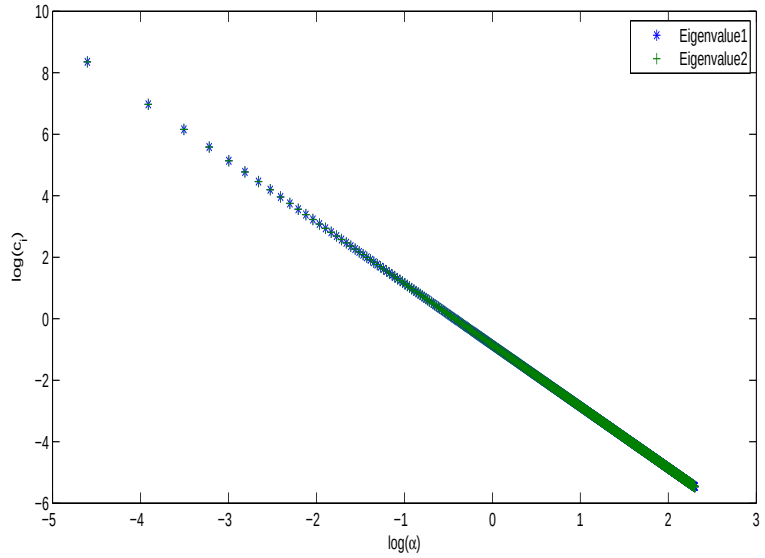

Figure 4.1: Imaginary parts of the eigenvalues function of $log(\alpha)$.

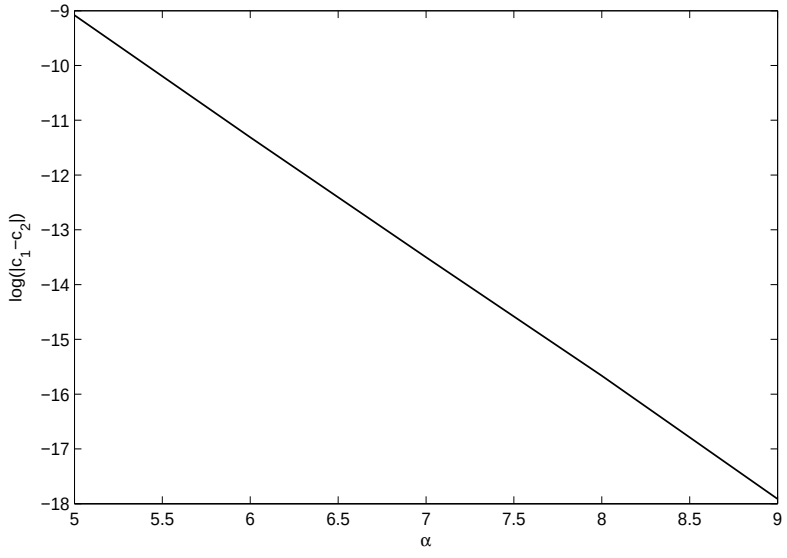

Figure 4.2: Difference between the eigenvalues for even and odd modes.

Table 4.1: Comparison of asymptotic and numerical results.

α	asymptotic approximation	eigenvalue 1	eigenvalue 2
5.0	0.346361±0.0340135i	0.344960±0.0320888i	0.344872±0.0320177i
6.0	0.296084±0.0236205i	0.295304±0.0225099i	0.295294±0.0225036i
7.0	0.258348±0.0173538i	0.257875±0.0166619i	0.257873±0.0166613i
8.0	0.229047±0.0132865i	0.228740±0.0128273i	0.228740±0.0128272i
9.0	0.205667±0.0104980i	0.205456±0.0101779i	0.205456±0.0101779i
10.0	0.186590±0.00850337i	0.186439±0.00827136i	0.186439±0.00827136i

Chapter 5

Conclusions and Perspectives

In this thesis, we have performed analysis to study the stability of few types of shear flows of viscoelastic fluids, specifically the plane Poiseuille and Couette flows, the hyperbolic-tangent shear layer, and the Bickley jet flows.

We focused on the upper-convected Maxwell model in the limit of infinite Weissenberg and Reynolds numbers. The stability differential equation is derived and solved numerically using the Chebyshev collocation spectral method. The algorithm has proven efficient in reproducing all the eigenvalues for the hydrodynamic stability and can be employed for other applications. The numerical solutions are compared with the analysis of the long and short wave limits and excellent agreements are shown. The main stability results are summarized as:

In the inviscid, non elastic case all profiles are unstable to long waves for free surface boundary conditions.

In the case of wall bounded flow no long wave instabilities were found for the plane Poiseuille and Couette flows. There are instabilities in the shear layer and the Bickley jet flows.

Another important feature we have found, is that an increase of the elasticity number has a stabilizing effect on all these flows. For some cases, this effect is not monotone, there are instances where a small amount of elasticity actually destabilizes the flow.

The linear stability in the short wave limit of shear flows bounded by two parallel free sur-

faces is also investigated. Unlike the plane Couette flow which has no short wave instability, we showed that plane Poiseuille flow has two unstable eigenmodes localized near the free surfaces which can be combined into an even and an odd eigenfunctions. The derivation of the asymptotic of these modes showed that our numerical eigenvalues are in agreement with the analytic formula and that the difference tends to zero exponentially. The imaginary part of the eigenvalue tends to zero like $1/\alpha^2$.

A number of unanswered questions are raised by this work and should be addressed in the future. A spatial analysis rather than a temporal analysis of the disturbance is possible; these are more relevant because it gives a more realistic representation of the transition to turbulence. We have only investigated the discrete spectrum rather than the continuous spectrum which improves our understanding of flow stability.

In the near future, I plan to study the flow stability of the upper-convected Maxwell model in the limit where both Reynolds and Weissenberg numbers are finite.

I will reexamine the equations governing the evolution of small disturbances in a viscous flow. The derivation of the stability equation follows the same path as outlined in our study. I can study the effects of viscosity, inertia, elasticity, and boundaries on the flow stability and understand the different types of the mechanisms that lead to instability. I would like to derive similar results for other types of flows and other geometries. Of course, having predicted these instabilities, I would like to see it experimentally verified.

There are other open stability problems which allow me to predict the onset of instability and draw some general features of the onset of chaos and turbulence. The theory of bifurcation and chaos provides a mathematical framework that can be used to understand qualitatively the transition to turbulence and the essence of instability of flows which may also be so complicated geometrically.

At high Reynolds numbers, shear flows arise in many applications in aero-and hydrodynamics. The flow around any obstacle or near a wall will develop steep velocity gradients close to the boundary because of the no-slip boundary conditions. These gradients dominate the frictional forces. In many industrial applications, polymers are added to high Reynolds number flows as a strategy to reduce frictional drag and hence to increase the volume flow

rate. The effect is used to enhance pipeline transport, decrease drag and noise production on submarines, stabilize water jets for fire fighting, among other things. The phenomenon requires flexible polymers and only arises when the flows become sufficiently turbulent, hence the name turbulent drag reduction. It has been shown to require an interaction between the time scales of the flow and the polymer [50]. The significance of the boundary layers for the drag then suggests that the drag reduction is due to a modification of the boundary layers. In the future I plan to build on previous work on instabilities in parallel shear flows, and insights into the relevance of coherent structures in shear flows and will apply it to the investigation of an idealized parallel boundary layer flow, the asymptotic suction boundary layer (ASBL). The usage of the ASBL allows me to connect coherent structure results in internal flows with turbulent phenomenology at higher Reynolds numbers and should open a path to a dynamical understanding of the effects of polymers.

Studies on three-dimensional flow structures have opened up another avenue to understanding the turbulence transition in flows with linear stability. The studies of Nagata (1992) and Busse and Clever (1992) on plane Couette flow and Faisst and Eckhardt (2003) on pipe flow have shown that below the transition to turbulence fully three-dimensional structures appear in the flow. Hof et al (2004) and Schneider et al (2007) in [51] show that these structures are also relevant in the temporally fluctuating turbulent state in that they appear transiently during the evolution of the flow. Typically, these structures consist of downstream vortices with transverse modulations. The modulations are essential, for translationally invariant structures can rigorously be shown to decay (Moffatt, 1990) in [52].

The transition between laminar and turbulent flows is controlled by edge states, structures that can be identified by the numercial method of 'edge state tracking' [51, 53, 54, 55, 56]. In spatially extended systems the edge states can also be localized [57, 58].

The impact of coherent structures on polymers has been studied by Graham et al. [60, 61, 62, 63, 64, 65]. They have identified changes in the characteristic scales and dynamics of the coherent structures as well as a polymer-induced intermittency in the flow.

The laminar boundary layer above a flat plat is described by the Blasius profile, with a thickness that increases like sqrt(x) in the downstream direction. The spatial development

of the boundary layer prevents a direct translation of the coherent structures discussed in the context of translationally invariant shear flows like plane Couette or pipe flow. A translationally invariant boundary layer flow is obtained in the presence of a constant cross flow. Experimentally, this can be realized with porous plates and steady suction [66].
The flow then develops an exponential boundary layer profile. Many of the transitional and dynamical properties are similar to the Blasius boundary layer. The advantage for a future study is that the translational invariance allows the direct transfer of the concepts from parallel shear flows to this boundary layer geometry, including studies of the turbulent dynamics and turbulent drag as well as the search for edge states and coherent structures and their bifurcations.
The polymer model most often implemented for the study of DR is the Finite Extensible Nonlinear Elastic model with Peterlin's closure (FENE P model). Although there are competing models (e.g., FENE, Oldroyd B), the FENE P model is preferred because it accounts for the finite extensibility of the molecule and uses a simple second-order closure model in the equation for the polymer stress tensor. The former characteristic, aside from being physically consistent with real polymers, reduces numerical instabilities, whereas the latter reduces computational costs. The FENE-P constitutive model can be used to capture the basic rheological properties of a polymer solution in many types of flows (Somasi et al. 2002, van Heel et al. 1998, Vincenzi et al. 2007, Wedgewood et al. 1991, Zhou, Akhavan 2003). I plan to implement the FENE-P model within the shear flow code 'Channelflow' which has been adapted to the ASBL geometry by G. Veble and T. Madre.
I then plan also to study a large range of rheological parameters (polymer length L, dimensionless Weissenberg number W, and polymer concentration). Below I present the steps of a possible future work:

1. I plan to investigate the elastic effects on the instability of the ASBL shear flows through a linear stability analysis. I will focus on FENE-P type constitutive model. The equation for stability will be derived and solved numerically using the spectral Chebyshev collocation method. The goal is to characterize the primary and secondary instabilities of the viscoelastic ASBL. I can also study the plane Couette flow within

channel flow, and then switch between the different flows and, in each case I expect significant viscoelastic stabilization of structures typically seen in Newtonian flows as it is shown in their simulations of high Reynolds number transition in the presence of viscoelasticity.

2. I will focus on coherent structures and their bifurcations. Edge states intermediate between laminar and turbulent can be found by direct adaption of the edge state tracking methods used for the Newtonian flows. For more general coherent structures I can use continuation techniques from plane Couette and Newtonian ASBL flows to obtain the viscoelastic counterparts.

3. I will study the viscoelastic effects for the turbulent asymptotic suction boundary layer (ASBL), including mean profiles, turbulent fluctuations and friction laws and global transport properties along the lines of the viscoelastic extension of the global transport properties described in Turbulent transport in Rayleigh-Benard, Taylor-Couette and pipe flows [67].

   The boundary layer equations for the evolution of the asymptotic suction boundary layer will be derived as well as the stability equations when the normal velocity is taken into account. The linear evolution of streamwise elongated structures triggered by a localized disturbance should be investigated. Two flows will be compared throughout the investigation, namely the asymptotic suction boundary layer (ASBL) and the Blasius boundary layer (BBL). I will set up a code for the ASBL, and another code for the full Blasius type boundary layer.

4. I will implement the polymers in channel flows, I will use John Gibson's Channelflow code and adapt it to the ASBL viscoelastic flows and extract more interesting information from it. Direct comparisons between the no suction (Blasius) and suction cases wil be made. I will see where the differences between the ASBL and real boundary layers are from Tobias Madre's results. Further theoretical studies of growth of streaky structures in the asymptotic boundary layer may give further information on the interpretation of the results. All I know is the dynamics of streaky structures holds the key

to much of the turbulent dynamics, so it will be good to see how the polymers influence streaks and vortices by changing their wavelength, amplitude and instabilities.

5. The turbulence simulations and interpretation of the nonlinear dynamics will be investigated. I will further study the mechanisms of instabilities by which polymers alter turbulence and reduce drag, I will be interested in the turbulent statistics, the boundary layers and the Reynolds stresses.

Bibliography

[1] A. Kaffel and M. Renardy. Surface modes in inviscid free surface shear flows, submitted to *Journal of Applied Mathematics and Mechanics* 2010

[2] J. Azaiez & G.M. Homsy, Linear Stability of free shear flow of viscoelastic liquids, *J. Fluid Mech.* **268** (1994), 37-69.

[3] P.G. Drazin & W.H. Reid, *Hydrodynamic Stability*, Cambridge University Press, Cambridge 1981.

[4] P.G. Drazin. *Introduction to Hydrodynamic Stability*, Cambridge University Press, Cambridge 2002.

[5] W. Heisenberg, Über Stabilität und Turbulenz von Flüssigkeitsströmen, *Ann. Phys.* **74** (1924), 577-627.

[6] R.G. Larson. Instabilities in viscoelastic flows, *Rheol. Acta* **31** (1992), 213-263.

[7] A purely elastic instability in Taylor-Couette flow R.G. Larson, Eric S. G. Shaqfeh and S. J. Muller. A purely elastic instability in Taylor-Couette flow. J. Fluid Mech., vol. 218, (1990), 573-800

[8] K.C. Lee & B.A. Finlayson. Stability of plane Poiseuille and Couette of a Maxwell fluid, *J. Non-Newt. Fluid Mech.* **21** (1986), 65-78.

[9] J.M. Rallison & E.J. Hinch, Instability of a high-speed submerged elastic jet, *J. Fluid Mech.* **288** (1995), 311-324.

[10] M. Renardy, Stability of viscoelastic shear flows in the limit of high Weissenberg and Reynolds numbers, *J. Non-Newt. Fluid Mech.* **155** (2008), 124-129.

[11] M.Renardy & Y. Renardy, Linear stability of plane Couette flow of an upper convected Maxwell fluid, *J. Non-Newt. Fluid Mech.* **22** (1986), 23-33.

[12] P.J. Schmid & D.S. Henningson, *Stability and Transition in Shear Flows*, Vol. 142 of Appl. Math. Sci., Springer, New York, 2001.

[13] E.S.G. Shaqfeh. Purely elastic instabilities in viscoelastic flows, *Ann. Rev. Fluid Mech.* **28** (1996), 129-185.

[14] R. Sureshkumar & A.N.Beris. Linear stability analysis of viscoelastic Poiseuille flow using an Arnoldi-based orthogonalization algorithm, *J. Non-Newt. Fluid Mech.* **56** (1995), 151-182.

[15] L.N. Trefethen. Spectral Methods in Matlab, *SIAM, Philadelphia, PA* (2000).

[16] Abramowitz M. & I. A.Stegun, Handbook of Mathematical Functions. *Dover.*(1965)

[17] Debler & Yu. The break-up of laminar liquid jets.*Proc. Roy. Soc London A* ***415****, 107–119* (1988).

[18] L. Hong & J.K Hunter. Singularity formation and instability in the unsteady inviscid and viscous Prandtl equations. *Comm. Math. Sci.* ***1****, 293–316* (2003).

[19] L.N. Howard. The number of unstable modes in hydrodynamic stability problems. *J. Mécanique* ***3****, 433–443* (1964).

[20] S.P. Lin. Breakup of Liquid Sheets and Jets. *Cambridge University Press* (2003).

[21] M. Renardy. Ill-posedness of the hydrostatic Euler and Navier-Stokes equations. *Arch. Rational Mech. Anal.* ***194****, 877–886* (2009a).

[22] M. Renardy. Short wave stability for inviscid shear flow. *SIAM J. Appl. Math.* ***69****, 763–768* (2009b).

[23] M. Renardy. *Mathematical Analysis of Viscoelastic Flows CBMS-NSF Regional Conference Series in Applied Mathematics* SIAM Philadelphia, (2000).

[24] A.L. Yarin. Free Liquid Jets and Films. *Hydrodynamics and Rheology. Longman* (1993).

[25] C.R. Doering, B. Eckhardt and J. Schumacher. Failure of energy stability in Oldroyd-B fluids at arbitrarily low Reynolds numbers, *J. Non-Newt. Fluid Mech.* **135** (2006), 92-96.

[26] R. Kupferman. On the linear stability of plane Couette flow for an Oldroyd-B fluid and its numerical approximation, *J. Non-Newt. Fluid Mech.* **127**(2005), 169-190.

[27] M. Renardy. Stressmodes in linear stability of viscoelastic flows, *J. Non-Newt. Fluid Mech.* **159** (2009), 137-140.

[28] T.C. Ho and M.M. Denn, J. Non-Newtonian Fluid Mech.3 (1977/78), pp.179.

[29] R.Rothenberger, D.H McCoy and M.M Denn, Flow instability in polymer melt extrusion, Trans. Soc. Rheol., 17 (1973) 259-269.

[30] K.C. Porteus and M.M Denn. Linear stability of plane Poiseuille flow of viscoelastic liquids, Trans. Soc. Rheol.,16 (1972) 295-308.

[31] V.A.Gorodtsov and A.I. Leonov. On a linear instability of a plane parallel Couette flow of viscoelastic fluid, J.Appl.Math. Mech., 31 (1967) 310-319.

[32] U. Akbay and G. Frischmann, Rheol. Acta 24 (1985) 450.

[33] U. Akbay and G. Frischmann, Z.angew Math. Mech. 65 (1985) T179.

[34] Alvarez, G. A., A. S. Lodge, and H.-J. Cantow, Measurement of the first and second normal stress differences: Correlation of four experiments on a polyisobutylene/decalin solution D1, Rheol. Acta 24, (1985) 368376.

[35] Magda J. J., Lou J., Baek SG, De Vries KL. Polymer. (1991) 32-2000.

[36] Bird RB, Curtiss CF, Armstrong RC, Hassager O. Dynamics of polymeric liquids, 2nd ed, vol 2. (1987) Wiley, New York

[37] Mackay ME, Boger DV . V. An explanation of the rheological properties of Boger fluids. J. Non-Newtonian Fluid Mech. 22 (1987), 235-243.

[38] Thomas, L.H. The stability of plane Poiseuille flow, Phys. Rev. 91(2) (1953), 780-783.

[39] Romanov, V.A. Stability of plane-parallel Couette flow. Funkcional Anal. i Prolozen 7(2), (1973), 62-73. Translated in Functional Analysis and Its Applications 7, 137-146.

[40] Tlapa, G. and Bernstein, B. Stability of a relaxation-type viscoelastic fluid with slight elasticity. Phys. Fluids 13,(1970) 565568.

[41] Gupta A.S. Stability of a visco-elastic liquid film flowing down an inclined plane. Journal of Fluid Mechanics (1967), Vol 28, 17-28 Cambridge University Press.

[42] Taylor, G.I. Stability of a viscous liquid contained between two rotating cylinders. Phil. Trans. Roy. Soc. London. A 223, (1923) 289-343

[43] Chandrasekhar, S. Hydrodynamic and Hydromagnetic stability (1961) Oxford University Press.

[44] G.H. McKinley, A. Oztekin, J.A. Byars, R.A. Brown. Self-similar spiral instabilities in elastic flows between a cone and a plate, J. Fluid Mech. 285 (1995) 123-164.

[45] D.O. Olagunju. Inertial effect on stability of cone-and-plate flow, J. Fluid Mech. 343 (1997) 317-330.

[46] Yuriko Renardy, David O. Olagunju. Inertial effect on stability of cone-and-plate flow Part 2: Non-axisymmetric modes. J. Non-Newtonian Fluid Mech., 78 (1998) 27-45

[47] Beard DW, Davies MH, Walters K. The stability of elastico-viscous flow between rotating cylinders Part 3. Overstability in viscous and Maxwell fluids. Journal of Fluid Mechanics (1966), 24: 321-334.

[48] S.J. Muller, R.G. Larson and E. S. G. Shaqfeh. A purely elastic transition in Taylor-Couette flow. Rheol Acta (1989) 28:499-503.

[49] D.W. Hughes, S.M. Tobias, On the instability of magnetohydrodynamic shear flows, Proc. R. Soc. Lond. A 457 (2001) 13651384.

[50] NS Berman, Drag reduction by polymers, Annu. Rev. Fluid Mech. 10 (1978) 47-64

[51] Schneider T.M, Eckhardt B, Vollmer J. Statistical analysis of coherent structures in transitional pipe flow. Phys. Rev. E. 75, 2007a 066313

[52] H.K. Moffatt. Fixed points of turbulent dynamical systems and suppression of nonlinearity. In Whither Turbulence? Turbulence at the Crossroads , Lecture Notes in Physics 357 (Springer-Verlag) 1990 pp 250257.

[53] Schneider T.M, Eckhardt B. Edge of chaos in pipe flow. Chaos. 16, (2006) 020604.

[54] Schneider T.M, Eckhardt B. Edge states intermediate between laminar and turbulent dynamics in pipe flow. Phil. Trans. R. Soc. A. 367, (2009) 577587.

[55] Schneider T.M, Eckhardt B, Yorke J.A. Turbulence transition and the edge of chaos in pipe flow. Phys. Rev. Lett. 99, 2007b 034502.

[56] Skufca J, Yorke J.A, Eckhardt B. The edge of chaos in a model for a parallel shear flow. Phys. Rev. Lett. 96, (2006) 174101.

[57] Mellibovsky F, Meseguer A. Critical threshold in pipe flow transition. Phil. Trans. R. Soc. A. 367, (2009) 545560.

[58] Tobias M. Schneider, Marinc, Eckhardt B. Localized edge states nucleate turbulence in extended plane Couette cells. Journal of Fluid Mechanics (2010), 646: 441-451.

[59] Alexander N. Morozov and Wim van Saarloos. Subcritical Finite-Amplitude Solutions for Plane Couette Flow of Viscoelastic Fluids. (2005) Phys. Rev. Lett. 95, 024501.

[60] Stone, P. A., Waleffe, F., and Graham, M. D., "Toward a structural understanding of turbulent drag reduction: nonlinear coherent states in viscoelastic shear flows," Phys. Rev. Lett. 89, 208301 (2002).

[61] Leslie Smith and Fabian Waleffe. Generation of slow large scales in forced rotating stratified turbulence , (2002) J. Fluid Mech., Vol. 451, pp. 145-168.

[62] Fabian Waleffe, J. Exact Coherent Structures in Channel Flow. J. Fluid Mech., Vol. 435, (2001) pp. 93-102.

[63] Li, W. Polymer induced drag reduction in exact coherent states of plane Poiseuille flow, Doctoral dissertation (2007).

[64] Li, W. and Graham, M. D. Polymer induced drag reduction in exact coherent structures of plane Poiseuille flow. Phys. Fluids, 19, 083101 (2007).

[65] Xi, L. and Graham, M. D. Turbulent drag reduction and multistage transitions in viscoelastic turbulent minimal flow units. J. Fluid Mech., 647, 421-452 (2010).

[66] Fransson,J. H. M. Experiments on stability, transition, separation and turbulence in boundary layer flows. (1992) KTH.

[67] B. Eckhardt, S. Grossmann and D. Lohse. Fluxes and energy dissipation in thermal convection and shear flows. EPL, 78 (2007) 24001.